# A developmentally defined population of neurons in the lateral septum controls responses to aversive stimuli

Miguel Turrero García[1,*], Diana N. Tran[2], Ralph E. Peterson[2], Sarah K. Stegmann[2], Sarah M. Hanson[1], Christopher M. Reid[1,3], Yajun Xie[1], Steve Vu[2], Corey C. Harwell[1,4,*]

[1]: Department of Neurology, University of California, San Francisco
[2]: Department of Neurobiology, Harvard Medical School
[3]: Ph.D. Program in Neuroscience, Harvard University
[4]: Lead contact
[*]: Authors for correspondence: miguel.turrerogarcia@ucsf.edu (M.T.G.), corey.harwell@ucsf.edu (C.C.H.)

## ABSTRACT

When interacting with their environment, animals must balance exploratory and defensive behavior to evaluate and respond to potential threats. The lateral septum (LS) is a structure in the ventral forebrain that calibrates the magnitude of behavioral responses to stress-related external stimuli, including the regulation of threat avoidance. The complex connectivity between the LS and other parts of the brain, together with its largely unexplored neuronal diversity, makes it difficult to understand how defined LS circuits control specific behaviors. Here, we describe a mouse model in which a population of neurons with a common developmental origin (*Nkx2.1*-lineage neurons) are absent from the LS. Using a combination of circuit tracing and behavioral analyses, we found that these neurons receive inputs from the perifornical area of the anterior hypothalamus (PeFAH) and are specifically activated in stressful contexts. Mice lacking *Nkx2.1*-lineage LS neurons display increased exploratory behavior even under stressful conditions. Our study extends the current knowledge about how defined neuronal populations within the LS can evaluate contextual information to select appropriate behavioral responses. This is a necessary step towards understanding the crucial role that the LS plays in neuropsychiatric conditions where defensive behavior is dysregulated, such as anxiety and aggression disorders.

## INTRODUCTION

The septum is a structure located in the mammalian ventral forebrain, between the lateral ventricles. It is subdivided into medial and lateral nuclei, each with distinct connectivity patterns and functions. The lateral septum (LS) controls different aspects of affective and motivated behavior through its complex connections to and from multiple other brain areas [1-4]. The LS has been classically subdivided into three nuclei (dorsal [LSd], intermediate [LSi], and ventral [LSv]), whose specific connectivity patterns and role in behavioral control vary along the rostro-caudal axis of the septum[2,3,5]. The septum is populated by multiple molecularly distinct neuron subtypes, although the true extent of their diversity is still unknown[2,6,7]. To understand how the septum controls specific behavioral responses, it is necessary to study defined neuronal populations and their connectivity. Developmental lineage is often a good predictor of mature neuron identity, as neurons with shared developmental origins tend to share aspects of their circuitry and functional features[7-11]. *Nkx2.1* is a transcription factor expressed during embryonic development in forebrain progenitors within the medial ganglionic eminence / preoptic area (MGE/PoA) and the septal eminence (SE); the latter proliferative area is distinguished as part of the developing septal complex by its expression of transcription factors of the Zic family[12-14]. Septal neurons within the *Nkx2.1*-lineage are derived primarily from progenitors located in the SE, and represent 10-30% of the total neuronal population in the mature septum[10]. Cholinergic *Nkx2.1*-lineage neurons in the medial septum are essential for normal learning and memory[8], but the role of SE-derived neuronal populations in the lateral septum has not been studied yet. In a recent study, we generated a mouse line where *Prdm16*, a gene encoding a transcriptional regulator, was deleted from cells with a developmental history of expression of *Nkx2.1*. This led to a decrease in the number of interneurons derived from the medial ganglionic eminence (MGE) in the cerebral cortex and other brain areas such as the hippocampus and the nucleus accumbens[15]. Here we report an almost complete ablation of *Nkx2.1*-lineage neurons in the lateral, but not the medial, septum. The majority of the missing LS cells were *Crhr2*-expressing neurons; in line with this, we found that mutant mice lacked a specific set of axonal inputs to the LS positive for the neuropeptide urocortin-3. These

axons originate from the perifornical area of the anterior hypothalamus (PeFAH) and normally form pericellular baskets onto LS *Nkx2.1*-lineage neurons. LS *Crhr2*-expressing cells drive stress-induced anxiety-like states and modulate threat responsivity[16,17]. We exposed mutant mice to a series of stress-inducing stimuli and found no evidence of general anxiety in mutant mice; rather, they exhibit increased preference for novel stimuli and exploratory behavior. Finally, we found that *Nkx2.1*-lineage neurons in the LSd are specifically activated by a stressful stimulus. Together, our data show that this population is responsive to stress, likely inhibiting exploratory drive in favor of defensive behavioral strategies when mice are under potential threat.

## RESULTS

### Deletion of *Nkx2.1*-lineage neurons in the lateral septum

*Nkx2.1*-lineage cells constitute a significant proportion of the medial and lateral septal nuclei[7,10,11]. Since newborn septal neurons express high levels of *Prdm16*[10], we decided to examine the effect of *Prdm16* deletion within the *Nkx2.1* lineage[15] in the septa of control (Nkx2.1Cre;Ai14, hereafter labeled as 'WT') and mutant (Nkx2.1Cre;Prdm16[f/f];Ai14, labeled as 'cKO') mice (**Figure 1A**). We discovered an almost complete absence of *Nkx2.1*-lineage cells (which could be identified by their expression of the fluorescent reporter tdTomato), from the lateral septum of cKO animals (**Figure 1B**). The density of tdTomato+ cells revealed a consistent loss of this population across three different positions along the rostro-caudal axis of the septum (with decreases of 92.9%, 93.8% and 83.0% in sections I, II and III, respectively; **Figures 1C,D; S1A**). This loss could be observed in all three subnuclei within the lateral septum (LSd, dorsal; LSi, intermediate; and LSv, ventral; **Figures 1B; S1B**), while the medial septum was unaffected (**Figure 1E**). In corresponding coronal sections, the area of the septum was reduced in both male and female mutant mice, particularly in posterior regions (**Figures 1F; S1D,E**). Since there was no decrease in the overall density of septal cells (identified by immunofluorescence for Zic-family proteins[10];

**Figure S1C**), this size reduction likely implies that the loss of *Nkx2.1*-lineage cells is not compensated by any other cell lineages. *Nkx2.1*-lineage cells in the septum comprise both neurons and astrocytes[10,18]; to determine that the cell ablation phenotype is specific to neurons, we performed immunofluorescence staining for the astrocyte marker SOX9 (**Figure S1F**), and found no difference in astrocyte density between WT and cKO samples, either in the LS or in the MS, where the majority of *Nkx2.1*-lineage astrocytes reside[7,10,18] (**Figure S1G**). Collectively, these results show that we have generated a genetic model wherein nearly all neurons with a history of *Nkx2.1* expression are specifically ablated in the lateral septum. This model provides the means to explore the involvement of lineage-defined neurons in the complex connectivity between the LS with other brain structures[1], and ultimately in the regulation of the innate behaviors controlled by those circuits[2,3].

## Reduced innervation of the lateral septum in the absence of *Crhr2*-expressing neurons

Based on the location and spatial distribution of *Nkx2.1*-lineage neurons in the mature LS, we hypothesized that they might overlap with a previously described population of neurons expressing the type 2 corticotropin-releasing hormone receptor, *Crhr2*[16,17,19]. We performed *in situ* hybridization for *Crhr2* and found an almost complete depletion of this mRNA throughout the LS of cKO mice (**Figure 2A**). We found that *Crhr2*-expressing cells were largely confined to the tdTomato+ *Nkx2.1*-lineage (**Figure 2B**), providing the first direct evidence that their developmental origin is the septal eminence[10]. The lateral septum is densely innervated by axons positive for urocortin-3 (UCN-3), a neuropeptide within the corticotropin-releasing factor family with high affinity for the CRHR2 receptor[20,21]. We reasoned that the absence of *Crhr2*-expressing neurons in the LS of cKO mice could result in altered distribution of axonal terminals containing UCN-3. As a first step to address potential circuit disruptions in cKO mice, we performed immunofluorescence staining for UCN-3 (**Figure 2C**). UCN-3 terminals densely innervated the LS of WT brains, forming perineuronal baskets around the somata of tdTomato+ neurons throughout all LS subnuclei (**Figures 2D,E; S2A**),

confirming the specificity of these inputs to *Nkx2.1*-lineage cells. UCN-3 terminals were largely absent from the LS of cKO mice (**Figure 2C**), and the rarely observed UCN-3+ baskets in these samples were not specific to the few remaining *Nkx2.1*-lineage cell (**Figure 2D,E**). We found a consistently reduced innervation in cKO samples, both in terms of fluorescence intensity (**Figure 2F**) and density of UCN-3 baskets (**Figure 2G**). This was the case for the three rostro-caudal positions that we analyzed, except for the LSv of the most rostral section (**Figure S2B**). We validated this observation using Enkephalin (Enk), another neuropeptide detected in axonal terminals throughout the LS and highly overlapping with UCN-3[6,22]. We compared immunofluorescence staining for Enk in WT and cKO brains (**Figure S2C,D**), finding a decrease in cKO samples that paralleled our observations for UCN-3 (**Figure S2E,F**). These concurrent observations provide compelling evidence of disrupted innervation of the lateral septum of cKO mice.

**PeFAH to LS inputs are lost in cKO mice**

We used monosynaptic retrograde circuit tracing to identify circuits specifically targeting *Nkx2.1*-lineage LS neurons and to better understand how septal connectivity might be disrupted in cKO brains. We performed stereotaxic injections using a combination of adeno-associated viruses and rabies viruses, enabling the labeling of neurons synapsing onto Cre-expressing cells (**Figure 3A**). Since *Nkx2.1* expression persists in the adult septum[23], we injected these viruses into the LS of Nkx2.1-Cre mice (**Figure S3A**). Subsequent analyses revealed the anatomical sources of synaptic inputs onto *Nkx2.1*-lineage neurons (summarized in **Figure 3B**). We detected labeled neurons in numerous brain regions previously described as the source of axonal terminals located in the LS[5] (**Figure 3C-F**). Many of these inputs came from the septal complex itself (both LS and MS/DBB) or from the hippocampus (especially areas CA1 in its most rostro-dorsal aspects, and CA3/CA1 in more caudo-ventral locations; **Figure 3E,F**). We also noted a smaller yet consistent proportion originating from other parts of the basal forebrain, including the hypothalamus (**Figure 3B**). Of these, we were particularly interested in the perifornical area of the anterior hypothalamus (PeFAH; **Figure 3D**). Previous studies have identified axonal terminals containing UCN-3, Enk, or both

neuropeptides in the LS, tracing their origin to neurons located in the PeFAH[5,22,24-28]. Since the afferents missing from the LS of cKO mice displayed a high overlap between UCN-3 and Enk signals (**Figure S2D**), they were likely to originate from this region. To verify this, we injected a retrograde circuit tracer (CTB-647, cholera toxin subunit beta conjugated with the fluorophore Alexa 647) into the LS of WT and cKO mice (**Figure 3G**). We identified retrogradely labeled neuronal cell bodies in the PeFAH of WT mice (**Figure 3H**), but not in cKO samples (**Figure 3I**). Other regions of the brain, such as the CA3 region of the hippocampus, were labeled by this technique in both genotypes (**Figure S3B,C**), pointing to a selective ablation of the PeFAH>LS circuit in mutant mice.

### *Nkx2.1*-lineage neurons are activated by acute restraint stress

Previous research has shown that *Crhr2*-expressing LS neurons, which largely overlap with the *Nkx2.1* lineage (**Figure 2A,B**), modulate behavioral responses to threatening stimuli when activated, producing an anxiety-like state when mice are exposed to persistent stress[16,17]. We decided to test whether an aversive stimulus would cause direct functional activation of this population. For this, we submitted WT and cKO mice to 30 minutes of forced restraint and analyzed the activation of neurons in the LS using immunofluorescence staining for c-Fos as a readout (**Figure 4A**). The lateral septum of animals submitted to forced restraint displayed numerous c-Fos+ cells, in both WT and cKO samples (**Figure 4B-D**). We quantified the density of c-Fos+ neurons throughout the LS along the dorsolateral axis, and found a robust increase in experimental animals, compared to the baseline in untreated mice (**Figures 4D, S4A,B**). As expected, the proportion of c-Fos+ cells belonging to the *Nkx2.1* lineage (i.e., tdTomato+) was consistently higher in WT than cKO brains in all LS subnuclei (**Figures 4C, S4C**). The proportion of *Nkx2.1*-lineage cells within the c-Fos+ population was significantly higher in animals subjected to forced restraint than in untreated controls (**Figure 4E**), even in cKO animals, where the overall proportion of tdTomato+ cells was much lower (**Figure S4D**). This increased proportion indicates that anxiogenic stimuli specifically activate *Nkx2.1*-lineage neurons in the lateral septum, consistent with the pattern of c-Fos staining in previous studies where animals were subjected to various anxiety-inducing

paradigms[29,30]. As a result of the ablation of this lineage, we observed a statistically significant reduction in the density of c-Fos+ neurons specifically in the LSd (**Figure 4F**), but not in the LSi or LSv of cKOs compared to WT (**Figure S4E**). These results demonstrate that a stressful stimulus activates LS *Nkx2.1*-lineage neurons, prompting us to investigate the behavioral consequences of deleting this population in cKO mice.

**Increased exploratory drive in cKO mice**

We next subjected control and mutant animals to a series of behavioral tests designed to assess general anxiety-like behavior in mice[16] (**Figure S5A-G**). Our results did not indicate a heightened or decreased anxiety status in cKO mice: we only observed significant differences between genotypes in the light-dark box and novel object paradigms: male cKO mice spent more time in the dark chamber in the former (**Figure S5B**), and more time exploring the novel object in the latter (**Figure S5D**). To compare the response of WT and cKO mice as they were faced with a more salient and aversive stimulus, we chose to perform a predator odor test, exposing mice to the smell of TMT (2,3,5-trimethyl-3-thiazoline), a component of fox odor that triggers an innate and strongly aversive response mediated by the lateral septum[30-32]. Mice were placed in an arena equipped with an air inlet, and the experiment consisted of two phases: an initial 15-minute habituation phase ('Blank phase'), similar to an open-field test, in which the arena was filled with air carrying a neutral odor. This was followed by a subsequent 15-minute test phase, during which the air in the arena contained the smell of TMT ('TMT phase') (**Figure 5A**). The behavior of mice throughout both phases was recorded with a depth sensor camera located above the center of the arena. Mice of both genotypes and sexes spent time exploring the novel stimulus (i.e., the air flow from the inlet) during the Blank phase, while they tended to move away from it during the TMT phase, as shown in the corresponding occupancy plots (**Figure 5B,C**). Interestingly, cKO mice continued to explore the air inlet during the TMT phase for longer than WT animals. This was reflected in the subtraction of Blank phase from TMT phase occupancy heatmaps (**Figure 5B**), but was only significantly different in females (**Figure 5C**). This suggests that, within this behavioral paradigm, novelty-triggered exploration can override anxiety-

induced aversion in female mutant mice. To further analyze behavioral differences between groups, we used MoSeq, an unsupervised automated behavior analysis pipeline[31]. This method detects sub-second behavioral motifs (or 'syllables') and quantifies their usage, facilitating unbiased comparisons across conditions to guide detailed analyses of behavior[31-33]. We observed certain emerging patterns when comparing the usage of each syllable in Blank *vs*. TMT phases within each genotype and sex. Syllables associated with ambulatory and/or exploratory behaviors (such as darting or rearing) were comparatively enriched during the Blank phase, while those related to stationary behavior (such as pausing or grooming) were used more often during the TMT phase (**Figure S5H-K**). This was consistent for both sexes and genotypes, and reflected our observations outlined above regarding the typical behavior that mice displayed during this experiment. We also compared syllable usage between WT and cKO mice in both the Blank and TMT phases, to assess the behavioral repertoire of each genotype in the absence and presence of a threatening stimulus. During the Blank phase, female WT mice displayed heightened vigilance, with increased frequencies of behavioral motifs such as jumping (syllable 26) and quick rearing (syllable 33). Conversely, female cKO animals differentially exhibited behaviors such as post-rearing ambulation (syllable 13) and prolonged, high rears (syllable 25), reflective of exploration (**Figure 5D**). In the TMT phase, animals of either genotype tended to use similar syllables differentially, suggesting that the heightened state of alert *vs*. exploration is consistent when comparing WT and cKO mice, respectively (**Figure 5E**). Male mice, despite their similarly strong response to TMT (**Figure S5J,K**), showed much more subtle differences in syllable usage between WT and cKO animals (**Figure S5L,M**). Taken together, the results from these experiments show that, while animals of both genotypes show threat avoidance behavior, cKO mice display an increased exploratory drive. This indicates that LS *Nkx2.1*-lineage neurons, informed by their inputs from the PeFAH, inhibit exploratory behavior when mice are faced with threatening stimuli, likely serving as a "brake" controlling the balance between exploration and avoidance in stressful contexts.

**DISCUSSION**

The lateral septum plays a central role in the regulation of numerous emotional and motivational behavioral states[1-3]. However, attributing particular aspects of behavioral control to distinct LS neuronal subpopulations has been challenging due to the incomplete understanding of LS neuronal diversity. Recent studies have focused on several molecularly defined groups of LS neurons to establish their involvement in social behavior[35,36] or context-specific defensive responses[16,17,37,38]. Our research complements these efforts, using a mouse model where *Crhr2*-expressing *Nkx2.1*-lineage neurons are absent from the lateral septum to assess the role of this subpopulation in the control of innate behavioral responses to stress-related stimuli. In line with previous research in the MS, we show that developmental origin is a strong predictor of septal neuron identity, and that lineage-based ablation of defined neuronal populations provides a valuable tool to test their function in the mature septum[8,11].

Deletion of *Prdm16* in *Nkx2.1*-expressing progenitors leads to the loss of approximately 30% of cortical interneurons derived from the MGE/PoA, whose function is partially compensated by other developmental lineages[15]. By contrast, septal eminence-derived *Nkx2.1*-lineage neurons in the LS appear to be especially susceptible to the loss of *Prdm16*, since it results in their almost complete ablation (**Figures 1, S1**). In the MGE/PoA, expression of *Prdm16* is confined to progenitors, where it controls their proliferative capacity[15]. In the developing septum, *Prdm16* expression is sustained in postmitotic neurons[10,39], potentially reflecting a specific need for this gene in the survival of septal neurons. The *Nkx2.1*-lineage in the LS is largely derived from the septal eminence, which produces sequential cohorts of neurons with diverse morphologies and anatomical locations over the neurogenic period[10]. This suggests that this lineage is composed of various neuron subtypes with distinct connectivity patterns and mature functions[2]. Besides their common developmental origin, mature *Nkx2.1*-lineage neurons share widespread expression of *Crhr2*, which in turn is largely confined to septal eminence-derived cells (**Figure 2**). The functional organization of cortical circuits depends heavily on the generation of diverse cell types that retain certain shared features based on their developmental origins[40]. Like the cortex, the lateral septum is

composed of diverse cell types derived from multiple progenitor domains[7,10,11]. The confluence of different developmental lineages within any given brain area is likely to be an evolutionary mechanism to refine and/or expand its circuitry and behavioral control. In the context of the *Nkx2.1*-lineage in the LS, future research should address the gene regulatory networks guiding the specification of neurons derived from the septal eminence, with special focus on the potential interplay between *Nkx2.1* and *Prdm16*.

We used a forced restraint assay to confirm the activation of LS *Nkx2.1*-lineage neurons as mice are exposed to stressful stimuli. As expected, we found a robust and consistent increase in the density of c-Fos+ neurons in the lateral septum of restrained mice[41-44], which was lower in cKO mice, particularly in the LSd. The proportion of activated *Nkx2.1*-lineage neurons was approximately doubled in restrained animals compared to controls, further confirming the involvement of this population in stress responses (**Figures 4, S4**). Acute restraint stress also activates PeFAH Ucn-3+[41] and AHN[44] neuronal populations, supporting the involvement of the PeFAH>LS>AHN circuit in response to anxiogenic stimuli. This circuit appears to be necessary to maintain the balance between defensive/avoidance behavior and exploratory drive, in line with the proven role of several other LS neuronal subpopulations and their circuitry in context-dependent risk assessment[16,17,37,38,42,45].

Currently, the lateral septum is regarded as a center that calibrates the intensity of behavioral responses to external stimuli, depending on context and on how and which of the complex intraseptal circuits are recruited[2,3]. The mouse model we describe here presents an opportunity to further understand how a subgroup of LS neurons regulates specific aspects of behavior. Based on a previous study that described the activity of *Crhr2*-expressing neurons as anxiogenic, we hypothesized that cKO mice, as they lack this population, would display lower levels of anxiety-related behaviors. However, we did not find clear differences in anxiety levels between WT and cKO mice using classic behavioral paradigms (**Figure S5**). The only significant results in these tests appear contradictory: more time spent on the dark chamber in the light-dark box test typically denotes heightened anxiety, while more time exploring the novel object in the

corresponding test is regarded as an indicator of reduced anxiety. However, these observations can be reconciled if we consider that mice were placed inside the light compartment of the light-dark box test during their daytime hours (see **Methods**). Both observed behaviors can be interpreted as an increase in the exploratory drive of cKO animals when faced with a novel stimulus, preferring the unfamiliar dark environment during daytime and showing a pronounced interest in a novel physical object within a familiar setting. The observed lack of preference for spatial novelty, as seen in the Y-maze test (**Figure S5G**), could reflect that this increase in exploratory behavior is dependent on the saliency of the stimulus. Using a different experimental paradigm, we observed an increased exploratory drive in cKO mice, reflected both in the greater amount of time they spent around the odor inlet and in their higher usage of exploration-related behavioral 'syllables' as revealed by MoSeq (**Figures 5, S5**). This effect was particularly clear in female mice, as opposed to the anxiety-related experiments, where we only observed significant results in male animals. This could be due to the increased variability in the exploratory behavior of individual male mice, which might obscure our MoSeq analyses in this specific context[34].

The lateral septum has been implicated in novelty-seeking behaviors in the past, mainly in the context of social novelty and in relation to its connectivity to other brain areas, such as the amygdala, prefrontal cortex and hypothalamus[46-48]. The disrupted connectivity that we observed, particularly the defective PeFAH>LS circuitry (**Figures 3, S3**), is one likely contributor to the increased exploratory drive of cKO mice. PeFAH Ucn-3 neurons are activated when mice engage in novelty exploration[49], while a neighboring GABAergic neuron population in the anterior hypothalamic nucleus (AHN) is activated during behavioral avoidance in anxiogenic contexts, including novel object approach and exposure to fox urine smell[50]. This population receives LS inputs, opening the possibility that *Nkx2.1*-lineage neurons are part of a PeFAH>LS>AHN circuit that could be responsible for risk assessment under stressful circumstances. The absence of PeFAH inputs to the LS in cKO animals would result in an impairment of long-range LS>AHN inhibition (either directly or through the complex intraseptal inhibitory sub-circuitry[2]), leading to a release of behavioral avoidance and increased exploratory drive.

This possibility is supported by evidence of *Crhr2*-expressing LS neuron efferent connections to the AHN[16,17]; however, further research is required to establish exact functional role of this circuit connection.

Our results fit with the current view of the lateral septum as a key component in the calibration of behavioral responses based on the motivational state and the external context of the animal[2,3]. We provide new insight into the connectivity and behavioral significance of the *Nkx2.1*-lineage/*Crhr2*-expressing LS neuronal population, establishing a novel model where it is almost entirely ablated. Our study highlights how understanding the developmental origin of different neuronal subtypes in the lateral septum can be an invaluable step towards understanding their mature identity and function.

## METHODS

## EXPERIMENTAL MODEL AND SUBJECT DETAILS

All animal procedures conducted in this study followed experimental protocols approved by the Institutional Animal Care and Use Committees of Harvard Medical School (HMS) and the University of California, San Francisco (UCSF). Mouse strains mentioned in the main text are listed in the **Key Resources** table. Mouse housing and husbandry were performed in accordance with the standards of the Harvard Medical School Center of Comparative Medicine (HCCM) at HMS, and the Laboratory Animal Resource Center (LARC) at UCSF. Mice were group housed in a 12 h light/dark cycle, with access to food and water *ad libitum*. Samples were obtained at the ages indicated in the Figure Legends and throughout the text. Results reported include animals of both sexes, balanced equally whenever possible, except where otherwise indicated.

## METHOD DETAILS
### Tissue processing for histology

Mice were transcardially perfused with PBS followed by 4 % paraformaldehyde (PFA) in 120 mM phosphate buffer; their brains were dissected out and post-fixed in 4 % PFA overnight at 4°C. Brains were sectioned into 50-100 $\mu$m sections on a vibratome and stored at -20°C in freezing buffer (30 % ethylene glycol, 28 % sucrose in 0.1 M sodium phosphate buffer), or at 4°C in PBS with 0.05 % sodium azide.

### Immunofluorescence

Floating vibratome sections were permeabilized with 0.5 % Triton X-100 in PBS for 1-2 h, then blocked with blocking buffer (10 % goat serum, 0.1 % Triton X-100 in PBS) for 1-2 h at room temperature. They were then incubated for 24-72 h, at 4°C, with primary antibodies diluted in blocking buffer. The samples were washed three times (10-30 min/wash) with PBS, counterstained with DAPI (4',6-diamidino-phenylindole) for 45 min (both steps at room temperature), and incubated with secondary antibodies diluted in blocking buffer for 2 h at room temperature or overnight at 4°C. They were then washed

(three 10-30 min washes) with PBS, and mounted on microscope slides with ProLong Gold Antifade Mountant.

**Fluorescent *in situ* hybridization**

50-$\mu$m sections were placed on slides and submitted to the RNAscope protocol (Advanced Cell Diagnostics), following the manufacturers' instructions with minor modifications. All RNAscope probes (as listed in the **Key Resources** table) were purchased from ACD.

**Microscopy and image analysis**

Images were acquired using either a Leica Stellaris laser point scanning confocal microscope or a Leica DM5500B widefield microscope. 10x, 20x and 40x objectives were used, and the parameters of image acquisition (laser intensity, speed, resolution, averaging, zoom, z-stack, etc.) were adjusted for each set of samples. Images were further analyzed using ImageJ, both in its native and Fiji distributions, as described below. Brightness and contrast were adjusted as necessary for visualization; the source images were kept unmodified.

**Cell quantification**. All cell type quantifications were done with the CellCounter tool in ImageJ/Fiji. All cells positive for the corresponding marker(s) within the dorsal, intermediate and ventral nuclei of the lateral septum (LSd, LSi, and LSv, respectively), as well as in the medial septal nucleus (MS) in **Figure 1E**, were counted. The rostro-caudal locations labeled as 'I', 'II', and 'III' throughout the manuscript correspond approximately to Bregma +0.75, +0.5 and +0.25, respectively.

**Septum size measurement**. For **Figures 1F and S1D**, 50- to 70-$\mu$m vibratome-sliced coronal sections corresponding to rostro-caudal sections I-III were measured. All sections had been subjected to immunofluorescence staining for other figures. The total area of the section and the area of the septum (defined as the part dorsal to a straight line drawn between the bottom corners of both lateral ventricles) were calculated in Fiji

after manually tracing them in the DAPI channel. The average proportion of septum/total section area of WT brains was used to normalize the measurements.

**Fluorescence intensity quantification**. For **Figures 2F, S2B and S2E**, the mean fluorescence intensity was calculated across the entirety of each area analyzed, using the 'Measure' tool in ImageJ, and then normalized by the background fluorescence level, which was calculated as the mean intensity of a 50 x 50 $\mu$m square located within the same area that presented no obvious urocortin-3 (**Figures 2F, S2B**) or enkephalin (**Figure S2E**) staining.

**Perineuronal basket quantification**. For **Figures 2E, 2G and S2F**, baskets were only quantified as such when the signal consistently surrounded at least 50 % of the perimeter of a neuron with visible DAPI counterstaining within the presumed soma. Examples are highlighted in **Figure 2D**.

**Stereotaxic injections**

All surgical procedures were performed under aseptic conditions and with appropriate analgesic treatment. Mice (2-6 months old) were anesthetized with isoflurane and placed on a stereotaxic apparatus (Kopf), while their temperature was maintained with a heating pad, and their eyes protected from drying with ophthalmic ointment. After hair removal and disinfection, an incision was made on the scalp to expose the cranium, which was perforated with a drill prior to injection. The coordinates used for injections were adjusted around a standard LSi target, set at AP +0.7 mm, ML ±0.47 mm, and DV -3.3 mm. Glass capillaries were front-filled with either virus or dye tracer (see below) and inserted into the brain tissue. After 5 minutes, the target volume of injection was delivered at a rate of 25 nl/s, using a nanoliter injector (WPI). The capillary was slowly drawn back 10 minutes after the injection. The incision was sutured, and mice were allowed to recover partially from anesthesia before being returned to a clean home cage. Their recovery post-surgery was monitored for a minimum of three days.

**Viral injections**. For monosynaptic retrograde labeling of inputs onto *Nkx2.1*-lineage neurons (**Figures 3A-F**, 50-150 nl of a helper virus (AAV8-hSyn-FLEX-TVA-P2A-eGFP-2A-oG, Salk Institute Viral Vector Core) were injected into the LS of Nkx2.1 Cre mice, followed 2-3 weeks later by 50 nl of a rabiesvirus (EnvA G-deleted Rabies-mCherry, Salk Institute Viral Vector Core). Mice were sacrificed 5-7 days after the second surgery.

**Dye injections.** For retrograde labeling of WT and cKO mice (**Figures 3G-I, S3B,C**), 50-150 nl of cholera toxin subunit B conjugated with Alexa Fluor 647 were injected into the LS. Mice were sacrificed 5-7 days after the injection.

**Behavior**

**Anxiety-related tests**

A series of tests were carried out to assess general anxiety-like behavior in WT *vs*. cKO mice. They were performed as described below, in the order laid out in **Figure S5A**: after an initial 2-week period of acclimation to the facilities of the Mouse Behavior Core at Harvard Medical School, mice were subjected to the light-dark box, open field and novel object tests, with one day in between tests; after 5 days to ten days, they were subjected to the elevated plus-maze and social interaction tests, with one day between both tests and another between the habituation and test portions of the second one; finally, after another period of one week to ten days, they were subjected to the Y-maze test. Experiments were conducted in three separate batches of 2-6 months old animals including WT, cKO, and heterozygote controls (Nkx2.1-Cre;Prdm16$^{+/f}$;Ai14+), from multiple litters. All mice were socially housed, with a minimum of 2 and a maximum of 5 littermates per cage. Male and female mice were tested separately, and the experimenters were blinded to the animals' genotypes until after the results were compiled. The experimental arenas were thoroughly cleaned (successively wiped with Windex and 70% ethanol) between individual tests.

**Light-dark box test.** The arena (open field chamber [ENV-510] with a dark box insert [ENV-511]; Med Associates) consisted of two equally-sized compartments connected by a small restricted opening. One of the compartments was brightly illuminated (700-800 lux), while the other remained in the dark. Mice were placed on the bright compartment and allowed to freely move within and between both chambers for 10 minutes. The number of entries and time spent in each compartment were recorded automatically using Activity Software (Med Associates). The measure compared in **Figure S5B** is % of the test time spent in the bright chamber.

**Open field test.** The arena was a uniformly illuminated box with a square (40x40 cm) base and an open top. Mice were placed in a corner of the box and allowed to freely move within it for 10 minutes. Their movements were recorded with a camera placed above the center of the arena, and analyzed using the Topscan software (CleverSys). The measure compared in **Figure S5C** is % of the test time spent in the center of the arena.

**Novel object test.** This test was performed and analyzed in the same arena and manner as the open field test, the only difference being the placement of a novel object (a small assembly of Lego pieces, approximately 4x4x7 cm in size) attached to the center of the base. The measure compared in **Figure S5D** is % of the test time spent in the middle of the arena.

**Elevated plus-maze test.** The arena consisted of two open and two (laterally) closed arms, all measuring 30 x 5 cm and extending from a central platform, located 85 cm above ground level. Mice were placed at the end of one of the open arms, facing the center, and allowed to freely explore the arena for 5 minutes in a dimly lit environment. Their movements were recorded with a camera placed above the center of the maze, and analyzed using the Topscan software (CleverSys). The measure compared in **Figure S5E** is % of the test time spent on the open arms.

**Social interaction test.** This test was performed on a three-chambered rectangular (62 x 40 cm) arena. The central chamber was separated from the side ones by restricted openings that could be blocked by removable doors. Each side chamber had a small perforated container located on a corner (in opposite locations). The test was performed in two phases, on two consecutive days. In the initial (habituation) phase, the test mouse was placed in the middle chamber, the doors to the side chambers were removed simultaneously and the subject was allowed to freely explore the arena for 10 minutes. In the second (test) phase, a "stranger" mouse (C57BL/6J strain, of the same sex as the test subject and with no prior contact with it) was placed under one of the perforated containers in the side chambers, and an object (the same Lego assembly that was used for the novel object test) under the other, in a random and counterbalanced way. Test mice were placed in the middle chamber and allowed to freely explore the arena for 10 minutes after removing the doors to the side chambers. Their movements were recorded and analyzed with the Topscan software (CleverSys). The measure compared in **Figure S5F** is the proportion of time spent in close proximity (within 2.5 cm) to the container where the unfamiliar mouse was placed, over the total amount of time spent exploring (i.e. close to) either container.

**Y-maze test.** This test was performed in a transparent Y-shaped arena enclosed on the sides, where two arms ("left" and "right") can be independently blockaded, with the third one serving as the starting arm. The arena was placed close to a large green holding rack, which served as a visual spatial cue for mice to differentiate the sides of the testing room. The test was run in two phases: during the habituation phase, either the left or the right arm was blockaded, and mice were placed at the end of the starting arm. They were allowed to freely explore the arena for 3 minutes, while their movements were recorded. They were then retrieved from the arena and placed in a designated empty cage, while the arena was cleaned and the blockade removed. During the test phase, the mice were put back into the maze in the same manner, and allowed to explore the arena for 3 minutes. Their movements were recorded and analyzed using the TopScan software (CleverSys). The measure compared in **Figure S5G** is the

proportion of time spent on the novel arm (i.e., the one that had been blockaded during the habituation phase) over the total amount of time spent on either "left" or "right" arms.

**Acute restraint stress**

Mice (6-7 months old) were placed inside 40 ml Falcon tubes with ventilation holes bored in at the tip (i.e. where the mouse's head was located). The tube caps were screwed in and the tubes were placed in a designated clean cage for 30 minutes. Mice were then removed from the tubes into their home cages, and sacrificed by transcardial perfusion 1 hour later. Male and female mice were subjected to restraint on different days, and the tubes were thoroughly cleaned with 70% ethanol and dry-wiped between subjects. Untreated age-matched controls were submitted to perfusion as described above, without any further experimental manipulations.

**Predator Odor Exposure**

A circular open field (US Plastics) with a small ⅛" diameter odor inlet on one side of the arena was used to expose animals for 15-minutes to a "blank" odor (dipropylene glycol), then 15-minutes of a 25% dilution of 2,3,5-trimethyl-3-thiazoline (TMT; diluted in dipropylene glycol). Filtered air (0.2-0.25 liters per minute) was blown over odorant-soaked filter paper (VWR) placed at the bottom of a Vacutainer syringe vial (Covidien). Independent PTFE tubing lines (Zeus) were used for blank and TMT sessions to avoid cross-contamination. All recordings were performed in darkness. The arena was cleaned with successive 70% ethanol – 10% bleach – 70% ethanol wiping steps and allowed to dry completely between subjects. Male and female mice were tested on different days.

**Occupancy Analysis.** Heatmaps (**Figure 5B**) were generated using the (x,y) centroid position of animals calculated during the extraction procedure. Specifically, a 2D histogram was generated using all data from both male and female datasets using the numpy (python) histogram2d() function with a bin size of 15. The specific x and y bin edges from this "grand" heatmap were used to generate all subsequent groupwise

heatmaps. To calculate the average heatmap for a given condition, a 2D histogram was generated for each session, normalized so that the histogram summed to 1, then appended to a (n_sessions x 15 bins x 15 bins) matrix. Finally, the average was taken across the first dimension to create a final (15x15) dimensional matrix. For heatmaps where differential occupancy is shown, average (15x15) heatmaps were simply subtracted from each other. For visualization purposes, all heatmaps were smoothed with a gaussian kernel using the matplotlib imshow() function. Odor inlet occupancy was quantified by computing the distance (vector norm) between the mouse centroid and a fixed odor port position, then counting the proportion of time the mouse spent closer to the odor port than a given threshold (40 mm in **Figure 5C**). Outliers (a total of four, one per sex and genotype) were identified by the Grubbs' test, performed online with the GraphPad Outlier calculator at https://www.graphpad.com/quickcalcs/grubbs1/, and excluded from statistical analyses.

**Motion Sequencing (MoSeq)**

**Data Acquisition.** Motion Sequencing (**Figures 5D,E, S5H-M**) is an unsupervised machine learning platform that segments continuous mouse behavior into its constituent parts, or behavioral "syllables"[32,51-53]. Data acquisition was performed as previously described[54]. Briefly, we used "depth" MoSeq, which operates on 3D data acquired by a depth sensor. Specifically, kinect2-nidaq software (https://github.com/dattalab/kinect2-nidaq) was used to acquire 3D images from a Kinect 2 depth camera at 30 Hz.

**MoSeq: Pre-processing, Data Extraction, Modeling.** Data was extracted, pre-processed, and modeled using the moseq2-app pipeline (https://github.com/dattalab/moseq2-app). Male and female mice used in this study had drastically different distributions of sizes; since MoSeq is sensitive to deviations of this magnitude, we separated male (1,669,346 frames) and female (1,346,820 frames) datasets for subsequent MoSeq analysis. In addition, the top/bottom 2.5% sized animals (mean mouse area) were omitted from each dataset, as detailed previously[34]. Default parameters were used for extraction and PCA. To determine an ideal value of

the hyperparameter kappa, a scan over a log range of 10 kappa values was performed on each dataset and a 100-iteration AR-HMM model was trained for each value of kappa. Following the kappa scan, the best kappa value (1,668,101 for both datasets) was selected using the Jensen-Shannon objective, which measures the similarity between the AR-HMM learned syllable duration distribution and the model-free changepoint duration distribution. A final 1000-iteration model was trained with a kappa of 1,668,101. The final model for each dataset had an overlapping syllable duration distribution and changepoint distribution similar to previously published datasets. All pre-processing, data extraction, and modeling were performed locally on a Windows 10 workstation.

**MoSeq: Analysis.** The moseq2-app pipeline was also used for syllable analysis. Syllables that accounted for 99% of variance explained were used for downstream analysis (53 for males, 53 for females). Using the interactive syllable labeling tool, syllables were given human labels by examining crowd movies. Differential syllable usage analysis was performed on all pairwise group comparisons for each dataset. Significantly different syllable usages were determined using a Kruskal-Wallis test, post-hoc Dunn's two-sided test with permutation, and multiple comparisons correction using the Benjamini-Hochberg procedure with a false discovery rate of 0.05[33]. All syllable usage error bars report the 95% confidence interval from 10,000-iteration bootstrapped syllable usages.

## Statistical analysis

Except for MoSeq (see above), all statistical analyses, as indicated in the corresponding Figure Legends, were performed using GraphPad Prism 9. All p-values were rounded to ten thousandth, and are presented above each statistical comparison in the corresponding figures; p-values below 0.05 (which we considered the cutoff for statistical significance) are highlighted in bold, while p-values deemed not statistically significant under this criterion are displayed in regular type within parentheses.

**KEY RESOURCES TABLE**

| REAGENT or RESOURCE | SOURCE | IDENTIFIER |
|---|---|---|
| **Antibodies** | | |
| Mouse monoclonal anti-Leu-Enkephalin | Abcam | Cat # ab150346 |
| Rabbit polyclonal anti-c-Fos | EnCor | Cat # RPCA-c-FOS |
| Chicken polyclonal anti-GFP | Aves | Cat # GFP-1020 |
| Mouse monoclonal anti-NeuN | Millipore | Cat # MAB377 |
| Rabbit polyclonal anti-RFP | Rockland | Cat # 600-401-379 |
| Goat polyclonal anti-Sox9 | RnD | Cat # AF3075 |
| Rabbit polyclonal anti-Urocortin-3 | Cosmo Bio | Cat # YII-Y364-EX |
| Rabbit polyclonal anti-ZIC | Segal Lab, DFCI[55] | N/A |
| Donkey polyclonal anti-goat Alexa 488 | Thermo Fisher | Cat # A11055 |
| Donkey polyclonal anti-rabbit 546 | Thermo Fisher | Cat # A10040 |
| Goat polyclonal anti-chicken Alexa 488 | Thermo Fisher | Cat # A11039 |
| Goat polyclonal anti-mouse Alexa 488 | Thermo Fisher | Cat # A11001 |
| Goat polyclonal anti-rabbit Alexa 488 | Thermo Fisher | Cat # A11008 |
| Goat polyclonal anti-rabbit Alexa 546 | Thermo Fisher | Cat # A11010 |
| Goat polyclonal anti-rat Alexa 647 | Thermo Fisher | Cat # A21247 |
| **Experimental Models: Organisms/Strains** | | |
| Mouse: B6.Cg-$Gt(ROSA)26Sor^{tm14(CAG-tdTomato)Hze}$/J (Ai14) | Jackson Laboratory | Stock no. 007914 |
| Mouse: C57BL/6J-Tg(Nkx2-1-cre)2Sand/J (Nkx2.1-Cre) | Jackson Laboratory | Stock no. 008661 |
| Mouse: B6.129-$Prdm16^{tm1.1Brsp}$/J ($Prdm16^{f/f}$) | Jackson Laboratory | Stock no. 024992 |
| **Bacterial and Virus Strains** | | |
| AAV8-hSyn-FLEX-TVA-P2A-eGFP-2A-oG | Salk Institute | Addgene 85225 |
| EnvA G-Deleted Rabies-mCherry | Salk Institute | Addgene 32636 |
| **Oligonucleotides** | | |
| RNAscope probe for *Crhr2* | ACD | Cat # 413201 |
| **Software and Algorithms** | | |
| Fiji 2.9.0/1.54e | Schindelin *et al.* 2012[56] | https://fiji.sc |
| Prism 9 | GraphPad | |

# ACKNOWLEDGEMENTS

## REFERENCES

1.  Sheehan, T.P., Chambers, R.A., and Russell, D.S. (2004). Regulation of affect by the lateral septum: implications for neuropsychiatry. Brain research. Brain research reviews *46*, 71-117. 10.1016/j.brainresrev.2004.04.009.

2.  Besnard, A., and Leroy, F. (2022). Top-down regulation of motivated behaviors via lateral septum sub-circuits. Mol Psychiatry. 10.1038/s41380-022-01599-3.

3.  Wirtshafter, H.S., and Wilson, M.A. (2021). Lateral septum as a nexus for mood, motivation, and movement. Neurosci Biobehav Rev *126*, 544-559. 10.1016/j.neubiorev.2021.03.029.

4.  Menon, R., Suss, T., Oliveira, V.E.M., Neumann, I.D., and Bludau, A. (2022). Neurobiology of the lateral septum: regulation of social behavior. Trends Neurosci *45*, 27-40. 10.1016/j.tins.2021.10.010.

5.  Risold, P.Y., and Swanson, L.W. (1997). Connections of the rat lateral septal complex. Brain research. Brain research reviews *24*, 115-195.

6.  Risold, P.Y., and Swanson, L.W. (1997). Chemoarchitecture of the rat lateral septal nucleus. Brain Res Brain Res Rev *24*, 91-113.

7.  Wei, B., Huang, Z., He, S., Sun, C., You, Y., Liu, F., and Yang, Z. (2012). The onion skin-like organization of the septum arises from multiple embryonic origins to form multiple adult neuronal fates. Neuroscience *222*, 110-123. 10.1016/j.neuroscience.2012.07.016.

8.  Magno, L., Barry, C., Schmidt-Hieber, C., Theodotou, P., Hausser, M., and Kessaris, N. (2017). NKX2-1 Is Required in the Embryonic Septum for Cholinergic System Development, Learning, and Memory. Cell reports *20*, 1572-1584. 10.1016/j.celrep.2017.07.053.

9.  Iyer, A., and Tole, S. (2020). Neuronal diversity and reciprocal connectivity between the vertebrate hippocampus and septum. Wiley Interdiscip Rev Dev Biol *9*, e370. 10.1002/wdev.370.

10. Turrero Garcia, M., Stegmann, S.K., Lacey, T.E., Reid, C.M., Hrvatin, S., Weinreb, C., Adam, M.A., Nagy, M.A., and Harwell, C.C. (2021). Transcriptional profiling of sequentially generated septal neuron fates. Elife *10*. 10.7554/eLife.71545.

11. Magno, L., Asgarian, Z., Apanaviciute, M., Milner, Y., Bengoa-Vergniory, N., Rubin, A.N., and Kessaris, N. (2022). Fate mapping reveals mixed embryonic origin and unique developmental codes of mouse forebrain septal neurons. Commun Biol *5*, 1137. 10.1038/s42003-022-04066-5.

12. Gaston-Massuet, C., Henderson, D.J., Greene, N.D., and Copp, A.J. (2005). Zic4, a zinc-finger transcription factor, is expressed in the developing mouse nervous system. Dev Dyn *233*, 1110-1115. 10.1002/dvdy.20417.

13. Inoue, T., Ota, M., Ogawa, M., Mikoshiba, K., and Aruga, J. (2007). Zic1 and Zic3 regulate medial forebrain development through expansion of neuronal progenitors. J Neurosci *27*, 5461-5473. 10.1523/JNEUROSCI.4046-06.2007.

14. Rubin, A.N., Alfonsi, F., Humphreys, M.P., Choi, C.K., Rocha, S.F., and Kessaris, N. (2010). The germinal zones of the basal ganglia but not the septum generate GABAergic interneurons for the cortex. J Neurosci *30*, 12050-12062. 10.1523/JNEUROSCI.6178-09.2010.

15.    Turrero Garcia, M., Baizabal, J.M., Tran, D.N., Peixoto, R., Wang, W., Xie, Y., Adam, M.A., English, L.A., Reid, C.M., Brito, S.I., et al. (2020). Transcriptional regulation of MGE progenitor proliferation by PRDM16 controls cortical GABAergic interneuron production. Development *147*. 10.1242/dev.187526.

16.    Anthony, T.E., Dee, N., Bernard, A., Lerchner, W., Heintz, N., and Anderson, D.J. (2014). Control of stress-induced persistent anxiety by an extra-amygdala septohypothalamic circuit. Cell *156*, 522-536. 10.1016/j.cell.2013.12.040.

17.    Hashimoto, M., Brito, S.I., Venner, A., Pasqualini, A.L., Yang, T.L., Allen, D., Fuller, P.M., and Anthony, T.E. (2022). Lateral septum modulates cortical state to tune responsivity to threat stimuli. Cell Rep *41*, 111521. 10.1016/j.celrep.2022.111521.

18.    Minocha, S., Valloton, D., Arsenijevic, Y., Cardinaux, J.R., Guidi, R., Hornung, J.P., and Lebrand, C. (2017). Nkx2.1 regulates the generation of telencephalic astrocytes during embryonic development. Sci Rep *7*, 43093. 10.1038/srep43093.

19.    Chalmers, D.T., Lovenberg, T.W., and De Souza, E.B. (1995). Localization of novel corticotropin-releasing factor receptor (CRF2) mRNA expression to specific subcortical nuclei in rat brain: comparison with CRF1 receptor mRNA expression. J Neurosci *15*, 6340-6350. 10.1523/JNEUROSCI.15-10-06340.1995.

20.    Li, C., Vaughan, J., Sawchenko, P.E., and Vale, W.W. (2002). Urocortin III-immunoreactive projections in rat brain: partial overlap with sites of type 2 corticotrophin-releasing factor receptor expression. J Neurosci *22*, 991-1001. 10.1523/JNEUROSCI.22-03-00991.2002.

21.    Lewis, K., Li, C., Perrin, M.H., Blount, A., Kunitake, K., Donaldson, C., Vaughan, J., Reyes, T.M., Gulyas, J., Fischer, W., et al. (2001). Identification of urocortin III, an additional member of the corticotropin-releasing factor (CRF) family with high affinity for the CRF2 receptor. Proc Natl Acad Sci U S A *98*, 7570-7575. 10.1073/pnas.121165198.

22.    Chen, P., Lin, D., Giesler, J., and Li, C. (2011). Identification of urocortin 3 afferent projection to the ventromedial nucleus of the hypothalamus in rat brain. J Comp Neurol *519*, 2023-2042. 10.1002/cne.22620.

23.    Magno, L., Catanzariti, V., Nitsch, R., Krude, H., and Naumann, T. (2009). Ongoing expression of Nkx2.1 in the postnatal mouse forebrain: potential for understanding NKX2.1 haploinsufficiency in humans? Brain Res *1304*, 164-186. 10.1016/j.brainres.2009.09.050.

24.    Szeidemann, Z., Shanabrough, M., and Leranth, C. (1995). Hypothalamic Leu-enkephalin-immunoreactive fibers terminate on calbindin-containing somatospiny cells in the lateral septal area of the rat. J Comp Neurol *358*, 573-583. 10.1002/cne.903580410.

25.    Merchenthaler, I. (1991). Co-localization of enkephalin and TRH in perifornical neurons of the rat hypothalamus that project to the lateral septum. Brain Res *544*, 177-180. 10.1016/0006-8993(91)90903-9.

26.    Onteniente, B., Menetrey, D., Arai, R., and Calas, A. (1989). Origin of the met-enkephalinergic innervation of the lateral septum in the rat. Cell Tissue Res *256*, 585-592. 10.1007/BF00225608.

27.    Horii-Hayashi, N., and Nishi, M. (2018). A Newly Defined Area of the Mouse Anterior Hypothalamus Involved in Septohypothalamic Circuit: Perifornical Area of the Anterior Hypothalamus, PeFAH. Acta Histochem Cytochem *51*, 1-8. 10.1267/ahc.17030.

28.    Ugur, M., Doridot, S., la Fleur, S.E., Veinante, P., and Massotte, D. (2021). Connections of the mouse subfornical region of the lateral hypothalamus (LHsf). Brain Struct Funct *226*, 2431-2458. 10.1007/s00429-021-02349-x.

29.    Duncan, G.E., Knapp, D.J., and Breese, G.R. (1996). Neuroanatomical characterization of Fos induction in rat behavioral models of anxiety. Brain Res *713*, 79-91. 10.1016/0006-8993(95)01486-1.

30.    Endres, T., and Fendt, M. (2008). Inactivation of the lateral septum blocks fox odor-induced fear behavior. Neuroreport *19*, 667-670. 10.1097/WNR.0b013e3282fb78d9.

31.    Wiltschko, A.B., Johnson, M.J., Iurilli, G., Peterson, R.E., Katon, J.M., Pashkovski, S.L., Abraira, V.E., Adams, R.P., and Datta, S.R. (2015). Mapping Sub-Second Structure in Mouse Behavior. Neuron *88*, 1121-1135. 10.1016/j.neuron.2015.11.031.

32.    Markowitz, J.E., Gillis, W.F., Beron, C.C., Neufeld, S.Q., Robertson, K., Bhagat, N.D., Peterson, R.E., Peterson, E., Hyun, M., Linderman, S.W., et al. (2018). The Striatum Organizes 3D Behavior via Moment-to-Moment Action Selection. Cell *174*, 44-58 e17. 10.1016/j.cell.2018.04.019.

33.    Gschwind, T., Zeine, A., Raikov, I., Markowitz, J.E., Gillis, W.F., Felong, S., Isom, L.L., Datta, S.R., and Soltesz, I. (2023). Hidden behavioral fingerprints in epilepsy. Neuron *111*, 1440-1452 e1445. 10.1016/j.neuron.2023.02.003.

34.    Levy, D.R., Hunter, N., Lin, S., Robinson, E.M., Gillis, W., Conlin, E.B., Anyoha, R., Shansky, R.M., and Datta, S.R. (2023). Mouse spontaneous behavior reflects individual variation rather than estrous state. Curr Biol *33*, 1358-1364 e1354. 10.1016/j.cub.2023.02.035.

35.    Shin, S., Pribiag, H., Lilascharoen, V., Knowland, D., Wang, X.Y., and Lim, B.K. (2018). Drd3 Signaling in the Lateral Septum Mediates Early Life Stress-Induced Social Dysfunction. Neuron *97*, 195-208 e196. 10.1016/j.neuron.2017.11.040.

36.    Li, L., Durand-de Cuttoli, R., Aubry, A.V., Burnett, C.J., Cathomas, F., Parise, L.F., Chan, K.L., Morel, C., Yuan, C., Shimo, Y., et al. (2023). Social trauma engages lateral septum circuitry to occlude social reward. Nature *613*, 696-703. 10.1038/s41586-022-05484-5.

37.    Besnard, A., Gao, Y., TaeWoo Kim, M., Twarkowski, H., Reed, A.K., Langberg, T., Feng, W., Xu, X., Saur, D., Zweifel, L.S., et al. (2019). Dorsolateral septum somatostatin interneurons gate mobility to calibrate context-specific behavioral fear responses. Nat Neurosci *22*, 436-446. 10.1038/s41593-018-0330-y.

38.    Azevedo, E.P., Tan, B., Pomeranz, L.E., Ivan, V., Fetcho, R., Schneeberger, M., Doerig, K.R., Liston, C., Friedman, J.M., and Stern, S.A. (2020). A limbic circuit selectively links active escape to food suppression. Elife *9*. 10.7554/eLife.58894.

39.    Kinameri, E., Inoue, T., Aruga, J., Imayoshi, I., Kageyama, R., Shimogori, T., and Moore, A.W. (2008). Prdm proto-oncogene transcription factor family expression and interaction with the Notch-Hes pathway in mouse neurogenesis. PloS one *3*, e3859. 10.1371/journal.pone.0003859.

40.    Fishell, G., and Kepecs, A. (2020). Interneuron Types as Attractors and Controllers. Annu Rev Neurosci *43*, 1-30. 10.1146/annurev-neuro-070918-050421.

41.    Horii-Hayashi, N., Sasagawa, T., Hashimoto, T., Kaneko, T., Takeuchi, K., and Nishi, M. (2015). A newly identified mouse hypothalamic area having bidirectional neural connections with the lateral septum: the perifornical area of the anterior hypothalamus

rich in chondroitin sulfate proteoglycans. Eur J Neurosci *42*, 2322-2334. 10.1111/ejn.13024.

42. Troyano-Rodriguez, E., Wirsig-Wiechmann, C.R., and Ahmad, M. (2019). Neuroligin-2 Determines Inhibitory Synaptic Transmission in the Lateral Septum to Optimize Stress-Induced Neuronal Activation and Avoidance Behavior. Biol Psychiatry *85*, 1046-1055. 10.1016/j.biopsych.2019.01.022.

43. Cullinan, W.E., Herman, J.P., Battaglia, D.F., Akil, H., and Watson, S.J. (1995). Pattern and time course of immediate early gene expression in rat brain following acute stress. Neuroscience *64*, 477-505. 10.1016/0306-4522(94)00355-9.

44. Sood, A., Chaudhari, K., and Vaidya, V.A. (2018). Acute stress evokes sexually dimorphic, stressor-specific patterns of neural activation across multiple limbic brain regions in adult rats. Stress *21*, 136-150. 10.1080/10253890.2017.1422488.

45. Zhong, C., Wang, L., Cao, Y., Sun, C., Huang, J., Wang, X., Pan, S., He, S., Huang, K., Lu, Z., et al. (2022). A neural circuit from the dorsal CA3 to the dorsomedial hypothalamus mediates balance between risk exploration and defense. Cell Rep *41*, 111570. 10.1016/j.celrep.2022.111570.

46. Rodriguez, L.A., Kim, S.H., Page, S.C., Nguyen, C.V., Pattie, E.A., Hallock, H.L., Valerino, J., Maynard, K.R., Jaffe, A.E., and Martinowich, K. (2023). The basolateral amygdala to lateral septum circuit is critical for regulating social novelty in mice. Neuropsychopharmacology *48*, 529-539. 10.1038/s41386-022-01487-y.

47. Chen, S., He, L., Huang, A.J.Y., Boehringer, R., Robert, V., Wintzer, M.E., Polygalov, D., Weitemier, A.Z., Tao, Y., Gu, M., et al. (2020). A hypothalamic novelty signal modulates hippocampal memory. Nature *586*, 270-274. 10.1038/s41586-020-2771-1.

48. de Leon Reyes, N.S., Sierra Diaz, P., Nogueira, R., Ruiz-Pino, A., Nomura, Y., de Solis, C.A., Schulkin, J., Asok, A., and Leroy, F. (2023). Corticotropin-releasing hormone signaling from prefrontal cortex to lateral septum suppresses interaction with familiar mice. Cell. 10.1016/j.cell.2023.08.010.

49. Horii-Hayashi, N., Nomoto, K., Endo, N., Yamanaka, A., Kikusui, T., and Nishi, M. (2021). Hypothalamic perifornical Urocortin-3 neurons modulate defensive responses to a potential threat stimulus. iScience *24*, 101908. 10.1016/j.isci.2020.101908.

50. Yan, J.J., Ding, X.J., He, T., Chen, A.X., Zhang, W., Yu, Z.X., Cheng, X.Y., Wei, C.Y., Hu, Q.D., Liu, X.Y., et al. (2022). A circuit from the ventral subiculum to anterior hypothalamic nucleus GABAergic neurons essential for anxiety-like behavioral avoidance. Nat Commun *13*, 7464. 10.1038/s41467-022-35211-7.

51. Wiltschko, A.B., Johnson, M.J., Iurilli, G., Peterson, R.E., Katon, J.M., Pashkovski, S.L., Abraira, V.E., Adams, R.P., and Datta, S.R. (2015). Mapping Sub-Second Structure in Mouse Behavior. Neuron *88*, 1121-1135. 10.1016/j.neuron.2015.11.031.

52. Wiltschko, A.B., Tsukahara, T., Zeine, A., Anyoha, R., Gillis, W.F., Markowitz, J.E., Peterson, R.E., Katon, J., Johnson, M.J., and Datta, S.R. (2020). Revealing the structure of pharmacobehavioral space through motion sequencing. Nat Neurosci *23*, 1433-1443. 10.1038/s41593-020-00706-3.

53. Weinreb, C., Osman, M.A.M., Zhang, L., Lin, S., Pearl, J., Annapragada, S., Conlin, E., Gillis, W.F., Jay, M., Ye, S., et al. (2023). Keypoint-MoSeq: parsing behavior by linking point tracking to pose dynamics. bioRxiv. 10.1101/2023.03.16.532307.

54.     Lin, S.G., W. F.; Weinreb, C.; Zeine, A.; Jones, S. C.; Robinnson, E.; Markowitz, J.; Datta, S. R. (2022). Characterizing the structure of mouse behavior using Motion Sequencing. arXiv. https://doi.org/10.48550/arXiv.2211.08497.

55.     Borghesani, P.R., Peyrin, J.M., Klein, R., Rubin, J., Carter, A.R., Schwartz, P.M., Luster, A., Corfas, G., and Segal, R.A. (2002). BDNF stimulates migration of cerebellar granule cells. Development *129*, 1435-1442.

56.     Schindelin, J., Arganda-Carreras, I., Frise, E., Kaynig, V., Longair, M., Pietzsch, T., Preibisch, S., Rueden, C., Saalfeld, S., Schmid, B., et al. (2012). Fiji: an open-source platform for biological-image analysis. Nat Methods *9*, 676-682. 10.1038/nmeth.2019.

## FIGURE LEGENDS

**Figure 1: A genetic model to ablate *Nkx2.1*-lineage neurons in the lateral septum.**
**A)** Coronal sections through the forebrain of postnatal day 30 (P30) control (labeled as 'WT'; Nkx2.1-Cre;Ai14, left) and mutant (labeled as 'cKO'; Nkx2.1-Cre;Prdm16flox/flox;Ai14, right) mice, where cells derived from Nkx2.1-expressing progenitors are labeled by the fluorescent reporter tdTomato (red). Nuclei are counterstained with DAPI (blue). Scale bars, 1 mm. **B)** Closeup of the septum of WT (left) and cKO (right) samples, as highlighted by white dashed line boxes in **A**. The main anatomical divisions of the mature septum are indicated by white dashed lines: medial septum (MS), lateral septum (LS), and dorsal (LSd), intermediate (LSi) and ventral (LSv) nuclei within the LS. Scale bar, 500 $\mu$m. **C)** Cartoon representing forebrain coronal sections at the three rostrocaudal positions used in subsequent analyses, and labeled as sections 'I', 'II' and 'III' throughout the article. The septal area is highlighted by red ellipses. **D)** Quantification of the density of cells positive for tdTomato per mm$^2$ in the lateral septum of WT (green circles, n = 9) and cKO (purple squares, n = 9) mice. **E)** Quantification of the density of cells positive for tdTomato per mm$^2$ in the medial septum of WT (green circles, n = 5) and cKO (purple squares, n = 5) mice. **F)** Quantification of the area of the septum relative to the total area of its corresponding coronal brain section in WT (green circles, n = 6) and cKO (purple squares, n = 5) male mice. Measurements are normalized to the corresponding WT average. Unpaired t-tests with Welch's correction were performed; the p-values are shown above the corresponding compared sets of data: bold typeface indicates statistically significant (p<0.05) differences.

**Figure 2: The absence of *Crhr2*-expressing neurons in cKO mice impairs the innervation of the lateral septum by Urocortin-3 axons. A)** Overview coronal images of the septum of P30 WT (left) and cKO (right) mice submitted to *in situ* hybridization for *Crhr2* (gray). Scale bars, 250 $\mu$m. **B)** Closeup view of the white dashed line boxes in **A**, showing the *Crhr2* signal (green) combined with immunofluorescence staining for tdTomato (magenta), in the LS of WT (top) and cKO (bottom) mice. Empty yellow arrowheads indicate examples of cells positive for both Crhr2 and tdTomato, while the cyan arrowhead highlights an example of a Crhr2+, tdTomato– cell. Scale bars, 50 $\mu$m. **C)** Overview coronal images of the septum of P30 WT (left) and cKO (right) mice submitted to immunofluorescence staining for urocortin-3 (gray). Scale bars, 250 $\mu$m. **D)** Closeup view of the white dashed line boxes in **C**, showing the urocortin-3 signal (UCN-3, green) combined with tdTomato (magenta), in the LS of WT (top) and cKO (bottom) mice. Empty orange arrowheads indicate examples of tdTomato+ cells surrounded by urocortin-3 perineuronal baskets, while the blue arrowhead shows a basket formed around a tdTomato– cell. Scale bars, 50 $\mu$m. **E)** Quantification of the proportion (in %) of urocortin-3 perineuronal baskets surrounding tdTomato+ cells in the LS of WT (green circles, n = 8) and cKO (purple squares, n = 7) mice at P30. **F)** Quantification of fluorescence intensity in the different LS subnuclei of P30 WT (green circles) and cKO (purple squares) brains where urocortin-3 was detected by immunofluorescence

staining. **G)** Quantification of the density of urocortin-3 baskets per mm$^2$ in the different LS subnuclei of P30 WT (green circles) and cKO (purple squares) mice. Unpaired t-tests with Welch's correction were performed; the p-values are shown above the corresponding compared sets of data: bold typeface indicates statistically significant (p<0.05) differences. **E**, **F** and **G** correspond to quantifications at the rostrocaudal level defined as section II in **Figure 1C**.

**Figure 3: Disrupted PeFAH to lateral septum connectivity in cKO mice. A)** Cartoon illustrating the experimental approach for retrograde monosynaptic circuit tracing from *Nkx2.1*-lineage neurons in the lateral septum. **B)** Graph summarizing the distribution of retrogradely labeled cells (represented as % of total mCherry+ cells) in the 10 main sources of synaptic inputs onto LS *Nkx2.1*-lineage cells. Squares represent male mice (n = 2), and circles female mice (n = 2). LS: lateral septum; MS/DBB: medial septum/diagonal band of Broca; PoA: preoptic area; LH: lateral hypothalamus; hyp: hypothalamus; CA1/2/3: Cornus Ammonis 1/2/3 regions of the hippocampus; Mamm: mammillary region; Thal: thalamus. **C-F)** Example images of retrogradely labeled neurons in different areas of the brain of an Nkx2.1-Cre mouse subjected to retrograde monosynaptic circuit tracing. The top panels show overview images stained for mCherry (red; expressed by neurons synapsing onto *Nkx2.1*-lineage cells in the LS) and counterstained with DAPI (blue); bottom panels show a closeup view of the areas highlighted by white dashed boxes in the overviews, displaying the mCherry channel (gray). The regions highlighted are: **C)** septum (lateral and medial); **D)** hypothalamus (PeFAH, perifornical area of the anterior hypothalamus); **E)** CA1 area in the rostro-dorsal hippocampus; **F)** CA1/CA3 area in the caudo-ventral hippocampus. Scale bars, 500 $\mu$m (overviews), 250 $\mu$m (closeups). **G)** Cartoon illustrating the experimental approach for retrograde circuit tracing in WT and cKO mice. CTB-647, cholera toxin beta subunit conjugated to Alexa-647 fluorophore. **H)** Representative image of the PeFAH of a WT mouse subjected to retrograde circuit tracing. Empty yellow arrowheads indicate the cell bodies of neurons labeled with CTB-647 injected into the LS (inset: injection site). PVN, periventricular nucleus of the hypothalamus. **I)** Representative image of the PeFAH of a cKO mouse subjected to retrograde circuit tracing (inset: injection site). Note the absence of CTB-647-labeled cell bodies. PVN, periventricular nucleus of the hypothalamus. Scale bars for **H** and **I**, 100 $\mu$m (main images), 500 $\mu$m (insets).

**Figure 4: *Nkx2.1*-lineage neurons in the LSd are activated by an acute stressful stimulus. A)** Experimental design: mice were subjected to 30 minutes of forced restraint and sacrificed 1 hour later; neurons firing in response to the anxiogenic stimulus were identified by immunofluorescence staining for c-Fos. Scale bars, 250 $\mu$m. **B)** Examples of coronal sections of the septum of WT (left) and cKO (right) mice after the forced restraint experiment, immunostained for c-Fos (green) and NeuN (blue). **C)** Closeup view of the white dashed line boxes in **B**, showing c-Fos (green) and tdTomato (magenta), in the different subnuclei within the LS of WT (left) and cKO (right) mice. Yellow arrowheads indicate examples of cells positive for both c-Fos and tdTomato;

cyan arrowheads highlight c-Fos+, tdTomato– cells, and the empty yellow arrowhead shows an example of a c-Fos–, tdTomato+ cell. Scale bars, 50 $\mu$m. **D)** Comparison of the density of c-Fos+ neurons in the LS of untreated controls ('baseline', empty symbols; n = 4 WT, green circles; n = 4 cKO, purple squares) and animals subjected to forced restraint ('restraint', full symbols; n = 4 WT, green circles; n = 4 cKO, purple squares). **E)** Proportion of tdTomato+ neurons within the c-Fos+ population in the LS of WT mice, comparing untreated controls ('baseline', empty circles, n = 4) and animals subjected to forced restraint ('restraint', full circles, n = 4). **F)** Comparison of the density of c-Fos+ neurons in the LSd of WT (green circles, n = 4) and cKO (purple squares, n = 4) animals subjected to forced restraint. Unpaired t-tests with Welch's correction were performed; the p-values are shown above the corresponding compared sets of data: bold typeface indicates statistically significant (p<0.05) differences.

**Figure 5: cKO mice display increased exploratory drive. A)** Experimental design: mice were placed in a cylindrical arena with a single odor inlet near the bottom, and exposed to two consecutive phases, where either a neutral (Blank) or an aversive (TMT) smell was pumped into the arena. **B)** Occupancy plots showing the average proportion of experiment time spent in each location throughout the arena by WT (n = 15 males, 13 females) or cKO (n = 14 males, 10 females) mice, under blank odor ("Blank") or anxiogenic ("TMT") conditions, as well as the difference between both plots ("cKO-WT"), separated by sex (top, males; bottom, females). **C)** Plot displaying the average occupancy of the area around the odor inlet (within a 40 mm radius) during Blank (gray triangles) and TMT (golden triangles) conditions, separated by sex and genotype. Each line joins the occupancy values of an individual mouse. Paired t-tests (Blank vs. TMT) and unpaired t-tests (WT vs. cKO) were performed; the p-values are shown above the corresponding compared sets of data: bold typeface indicates statistically significant (p<0.05) differences. **D)** MoSeq-generated syllable usage in female mice during the Blank portion of the experiment, with syllables most enriched in cKO mice to the left, and in WT to the right. **E)** Syllable usage in female mice during the TMT portion of the experiment, with syllables most enriched in cKO mice to the left, and in WT to the right. Data points in **D** and **E** represent the average ± 95% confidence interval of the proportion (in %) of test time spent using the corresponding syllable. Significantly different syllable usage (indicated by asterisks) was determined using a Kruskal-Wallis test, post-hoc Dunn's two-sided test with permutation, and multiple comparisons correction using the Benjamini-Hochberg procedure with a false discovery rate of 0.05.
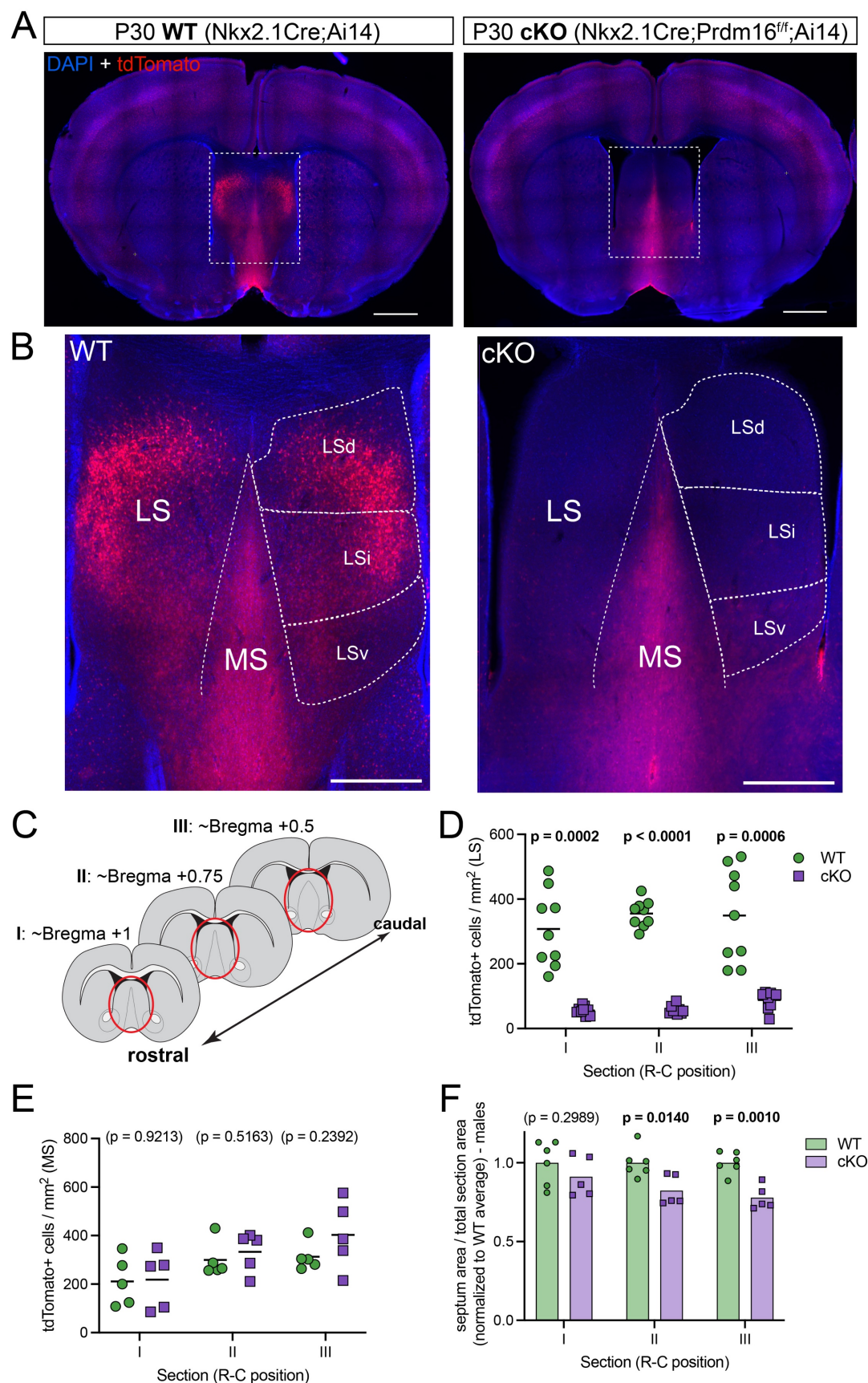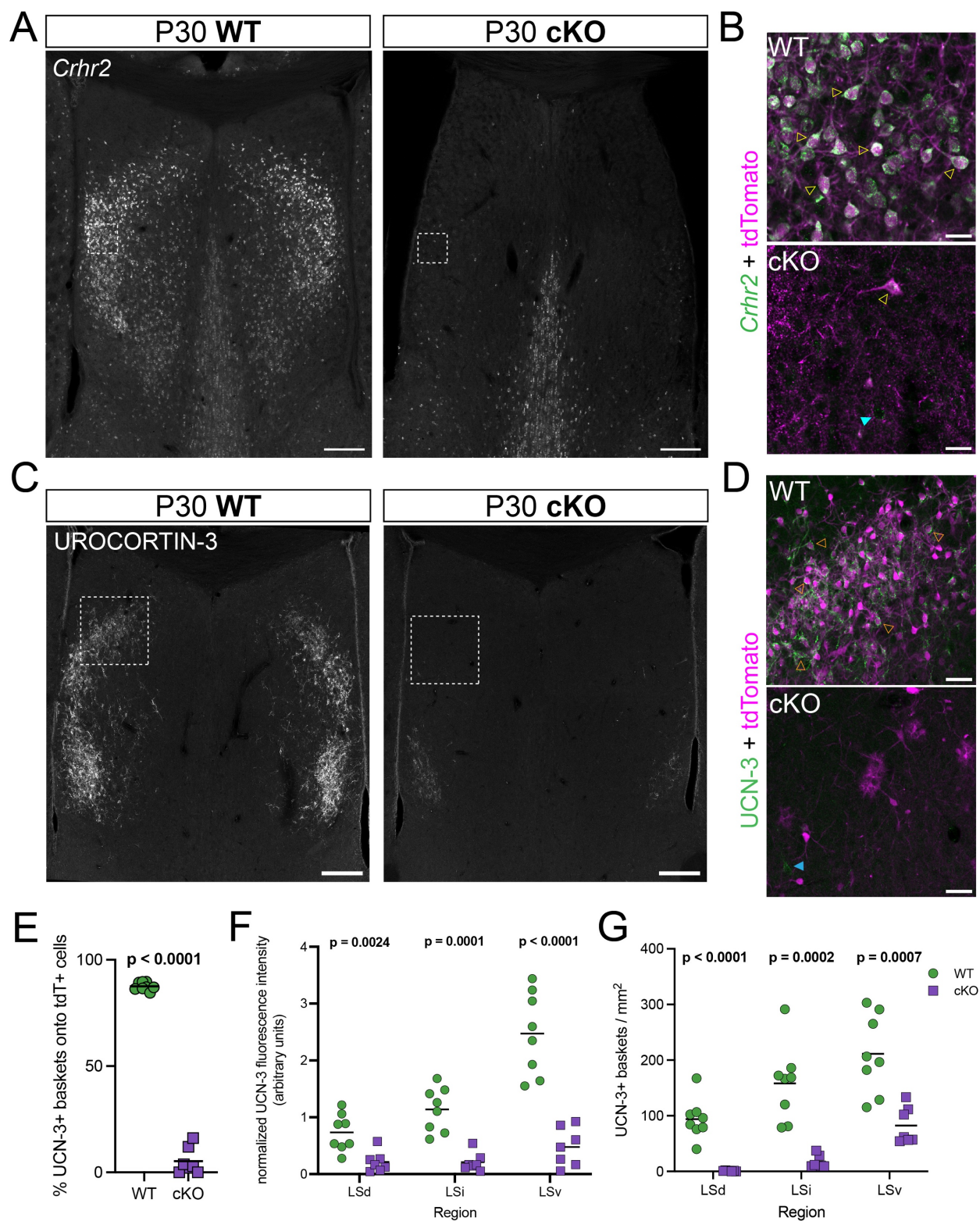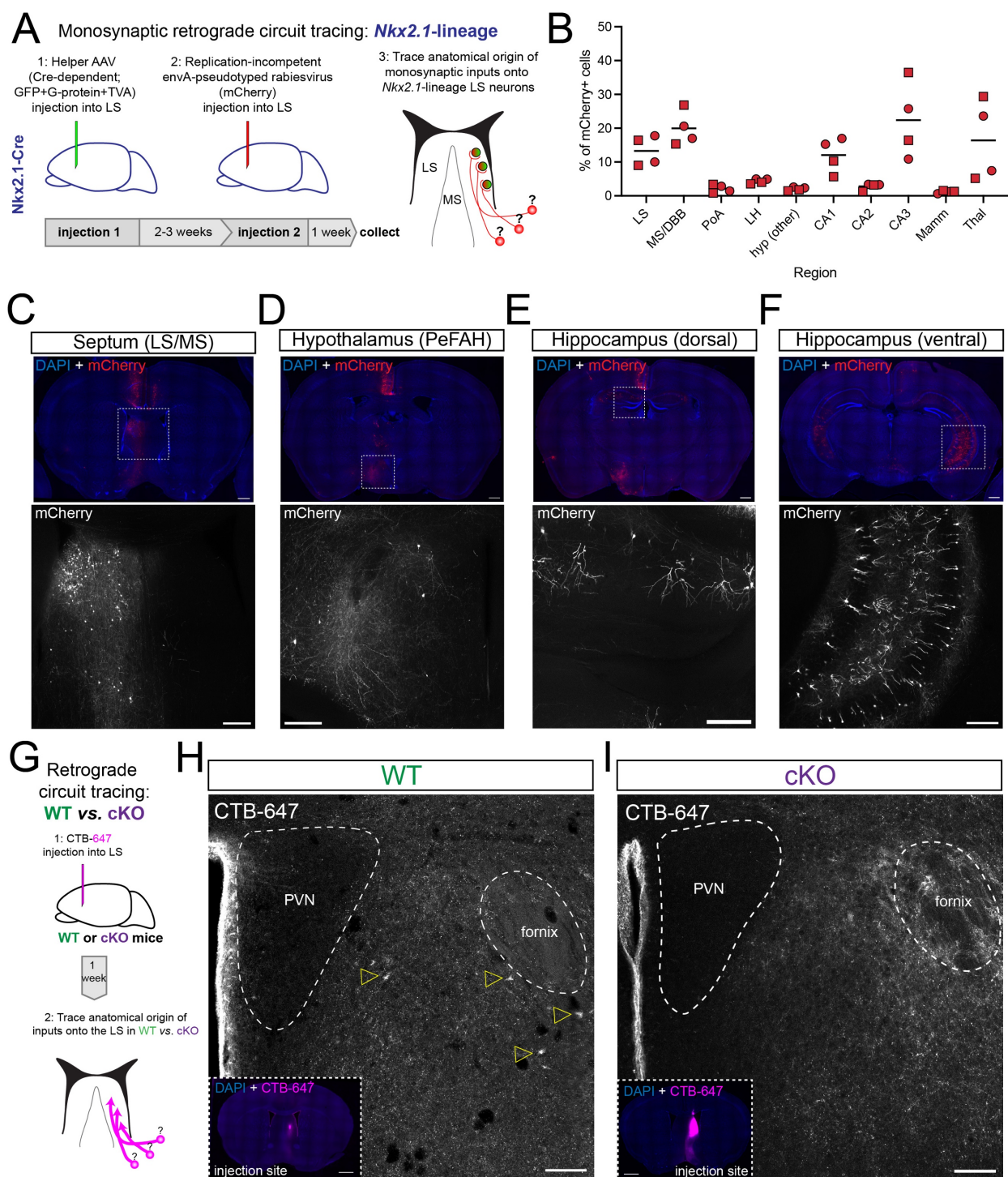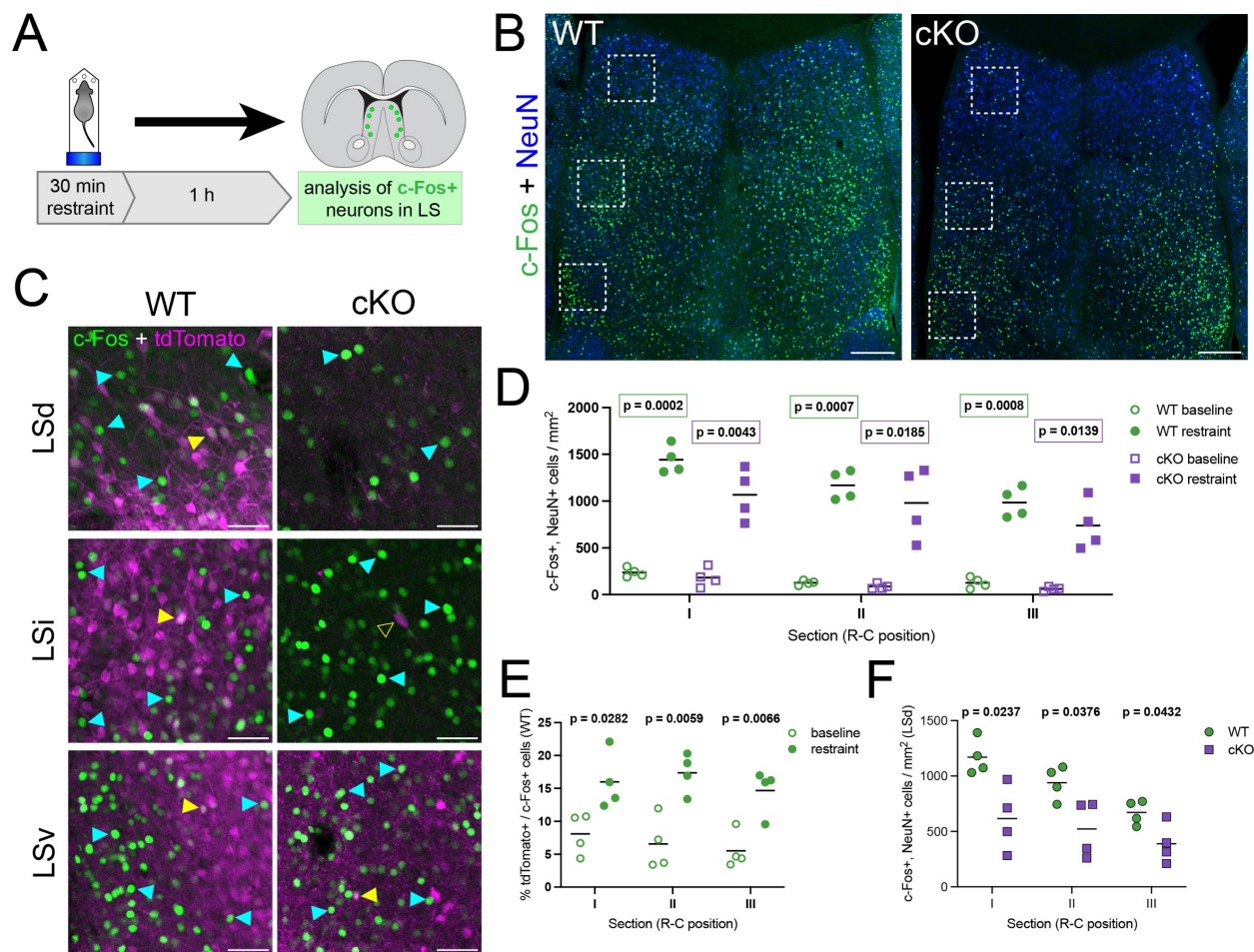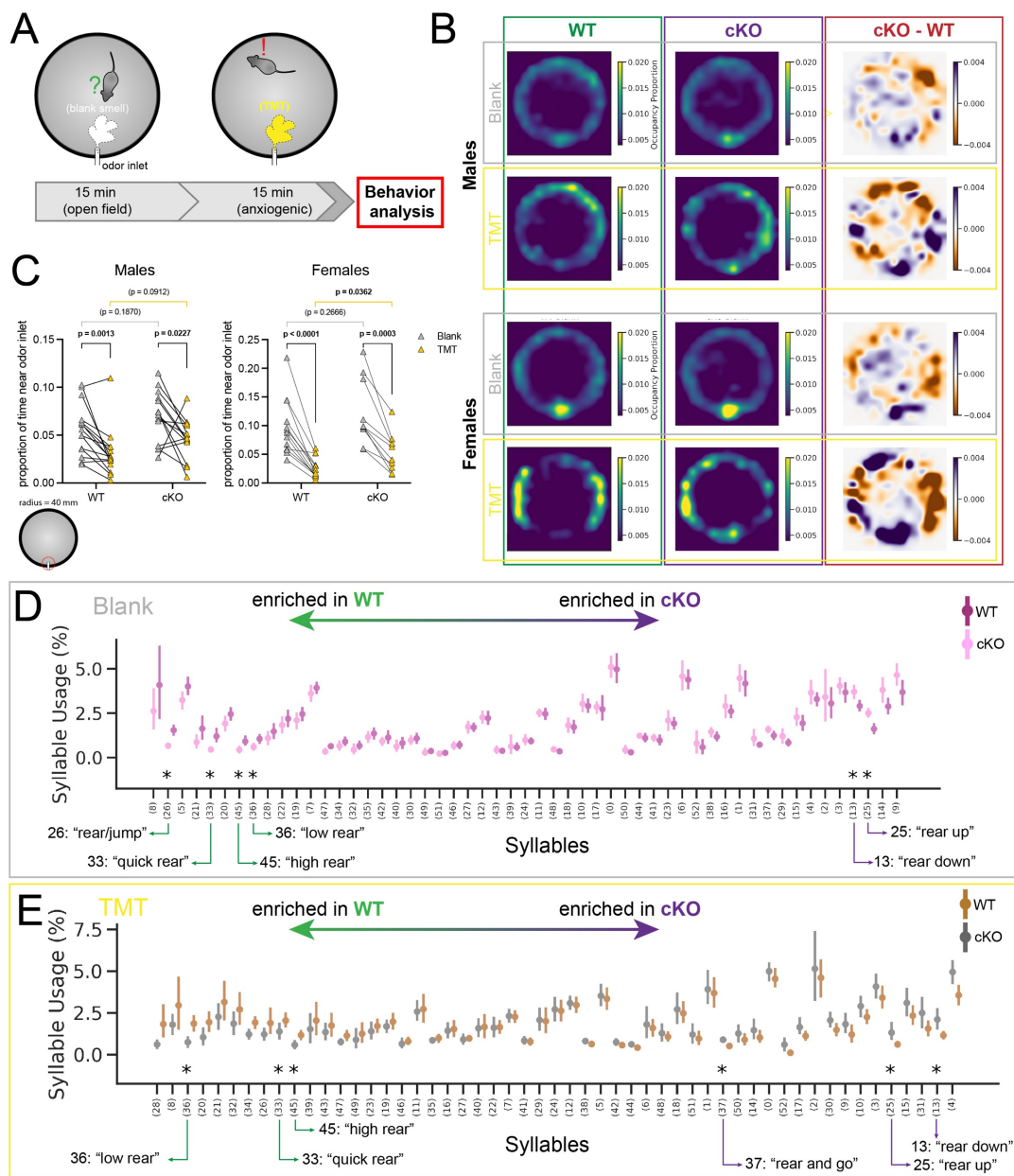
# Figure 1

# Figure 2

# Figure 3

# Figure 4

# Figure 5

## SUPPLEMENTARY FIGURE LEGENDS

**Figure S1, related to Figure 1. A)** Coronal sections along the rostral (left) to caudal (right) axis through the forebrain of P30 WT (top) and cKO (bottom) mice, submitted to immunofluorescence staining for tdTomato (magenta) and counterstained with DAPI (blue). Scale bars, 250 $\mu$m. **B)** Quantification of the density of cells positive for tdTomato per mm$^2$ in the different subnuclei within the lateral septum of WT (green circles, n = 9) and cKO (purple squares, n = 9) mice. LSd, dorsal lateral septum; LSi, intermediate lateral septum; LSv, ventral lateral septum. **C)** Quantification of the density of cells positive for Zic per mm$^2$ in the lateral septum of WT (green circles, n = 4) and cKO (purple squares, n = 4) mice. **D)** Quantification of the area of the septum relative to the total area of its corresponding coronal brain section in WT (green circles, n = 6) and cKO (purple squares, n = 5) female mice. Measurements are normalized to the corresponding WT average. **E)** Quantification of the density of cells positive for tdTomato per mm$^2$ in the lateral septum of WT (green symbols, n = 5 males, 4 females) and cKO (purple symbols, n = 5 males, 4 females) mice, as in **Figure 1D**, separated by sex as indicated. **F)** Example images of the septa of P30 WT (left) and cKO (right) mice, submitted to immunofluorescence staining for Sox9 (green) and counterstained with DAPI (blue). Scale bars, 250 $\mu$m. **G)** Quantification of the density of cells positive for Sox9 per mm$^2$ in the lateral (left) and medial (right) septum of WT (green circles, n = 4) and cKO (purple squares, n = 4) mice. Unpaired t-tests with Welch's correction were performed; the p-values are shown above the corresponding compared sets of data: bold typeface indicates statistically significant (p<0.05) differences.

**Figure S2, related to Figure 2. A)** Quantification of the proportion (in %) of urocortin-3 perineuronal baskets surrounding tdTomato+ cells in the different subnuclei within the LS of WT (green circles, n = 8) and cKO (purple squares, n = 7) mice at P30. **B)** Quantification of fluorescence intensity in the different LS subnuclei of P30 WT (green circles, n = 8) and cKO (purple squares, n = 7) brains where urocortin-3 was detected by immunofluorescence staining, at the Section I and Section III levels along the rostrocaudal axis. **C)** Overview coronal images of the septum of P30 WT (left) and cKO (right) mice submitted to immunofluorescence staining for enkephalin (gray). Scale bars, 250 $\mu$m. **D)** Closeup view of the white dashed line boxes in **C**, showing the combined signals for enkephalin (green) and urocortin-3 (magenta), in the LS of WT (top) and cKO (bottom) mice. Scale bars, 50 $\mu$m. **E)** Quantification of fluorescence intensity in the different LS subnuclei of P30 WT (green circles, n = 8) and cKO (purple squares, n = 7) brains where enkephalin was detected by immunofluorescence staining, at three levels along the rostrocaudal axis (Sections I through III). **F)** Quantification of the density of enkephalin+ baskets per mm$^2$ in the different LS subnuclei, at three levels along the rostrocaudal axis (Sections I through III), in WT (green circles; n = 8, n = 5 and n = 5 for Sections I, II and III, respectively) and cKO (purple squares; n = 5, n = 4 and n = 3 for Sections I, II and III, respectively) mice. Unpaired t-tests with Welch's correction were performed; the p-values are shown above the corresponding compared sets of data: bold typeface indicates statistically significant (p<0.05) differences.

**Figure S3, related to Figure 3. A)** Example of injection site in the lateral septum of an Nkx2.1-Cre mouse subjected to retrograde monosynaptic circuit tracing, stained for GFP (green; expressed by *Nkx2.1*-lineage cells infected by the helper AAV) and counterstained with DAPI (blue). Scale bar, 500 *µ*m. **B,C)** Examples of retrogradely labeled neurons in the ventral hippocampus of WT (**B**) and cKO (**C**) brains (corresponding to the same animals displayed in **Figure 3H** and **I**, respectively) injected with CTB-647 into the lateral septum. Scale bars, 250 *µ*m.

**Figure S4, related to Figure 4. A)** Examples of coronal sections of the septum of WT (left) and cKO (right) age-matched control mice (i.e., not subjected to the forced restraint experiment), immunostained for c-Fos (green) and counterstained with DAPI (blue). **B)** Quantification of the density of c-Fos+ neurons per mm$^2$ in the entire LS of WT (green circles, n = 4) and cKO (purple squares, n = 4) control animals. **C)** Proportion of tdTomato+ neurons within the c-Fos+ population in the different subnuclei within the LS of WT (green circles, n = 4) and cKO (purple squares, n = 4) mice subjected to forced restraint. **D)** Proportion of tdTomato+ neurons within the c-Fos+ population in the LS of cKO mice, comparing untreated controls ('baseline', empty squares) and animals subjected to forced restraint ('restraint', full squares). **E)** Comparison of the density of c-Fos+ neurons in the LSi (top) and the LSv (bottom) of WT (green circles) and cKO (purple squares) animals subjected to forced restraint. Unpaired t-tests with Welch's correction were performed; the p-values are shown above the corresponding compared sets of data: bold typeface indicates statistically significant (p<0.05) differences.

**Figure S5, related to Figure 5. A)** Overview of the timeline used when performing anxiety-related behavior tests. **B-G)** Left, cartoons illustrating the outline of each behavior test; right, summary of the main anxiety-related readout for males and females. The behavioral tests performed were: **B**, light-dark box; **C**, open field; **D**, novel object; **E**, elevated plus-maze; **F**, social interaction; **G**, Y-maze. Unpaired t-tests with Welch's correction were performed; the p-values are shown above the corresponding compared sets of data: bold typeface indicates statistically significant (p<0.05) differences. **H, J)** Syllable usage in female (**H**) and male (**J**) WT mice during both parts of the experiment, with syllables most enriched in the TMT portion to the left, and in the Blank portion to the right. **I, K)** Syllable usage in female (**I**) and male (**K**) cKO mice during both parts of the experiment, with syllables most enriched in the TMT phase to the left, and in the Blank phase to the right. **L)** Syllable usage in male mice during the Blank portion of the experiment, with syllables most enriched in cKO mice to the left, and in WT to the right. **M)** Syllable usage in male mice during the TMT portion of the experiment, with syllables most enriched in cKO mice to the left, and in WT to the right. Data points in **H-M** represent the average ± 95% confidence interval of the proportion (in %) of test time spent using the corresponding syllable. Significantly different syllable usage (indicated by asterisks) was determined using a Kruskal-Wallis test, post-hoc

Dunn's two-sided test with permutation, and multiple comparisons correction using the Benjamini-Hochberg procedure with a false discovery rate of 0.05.
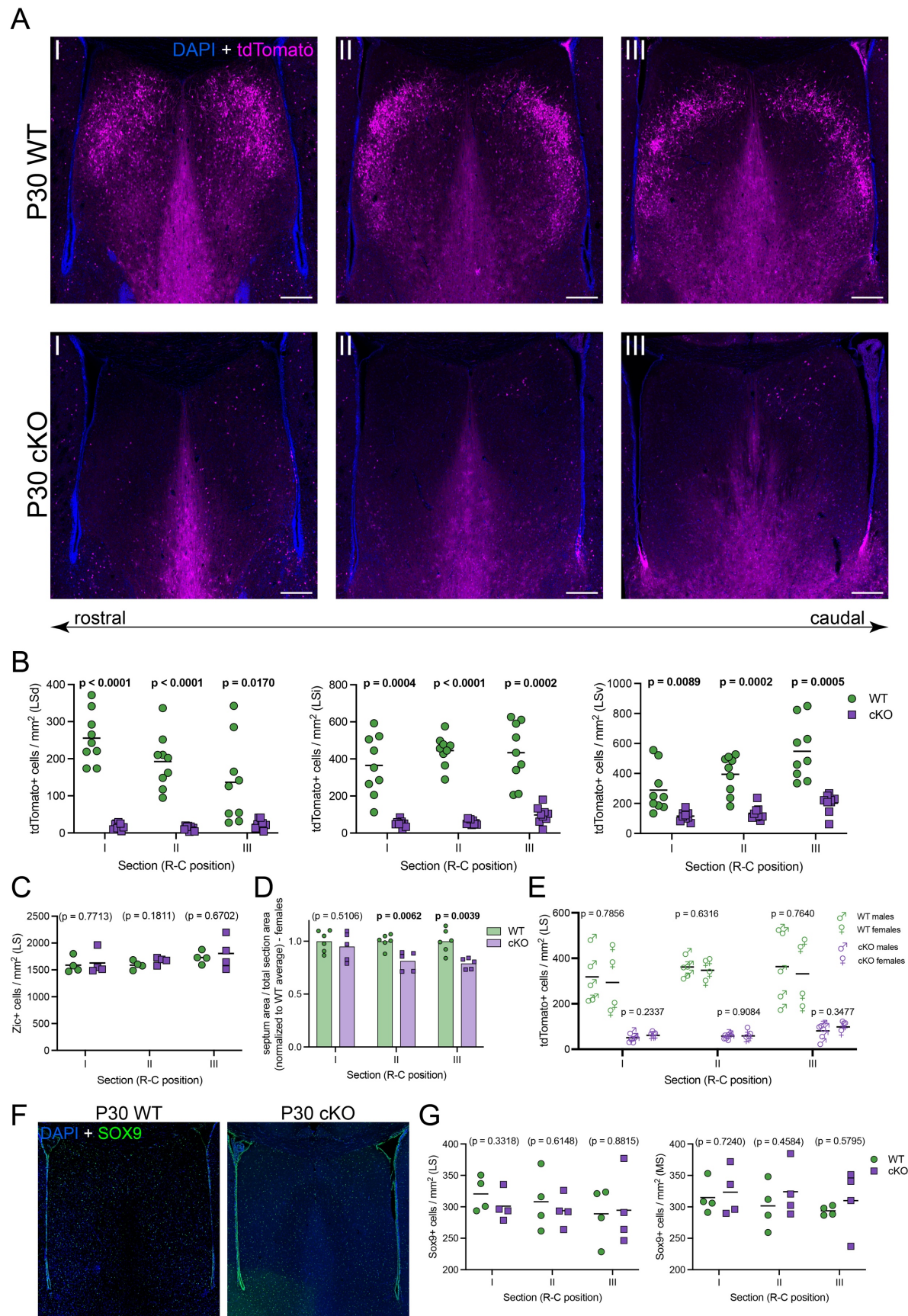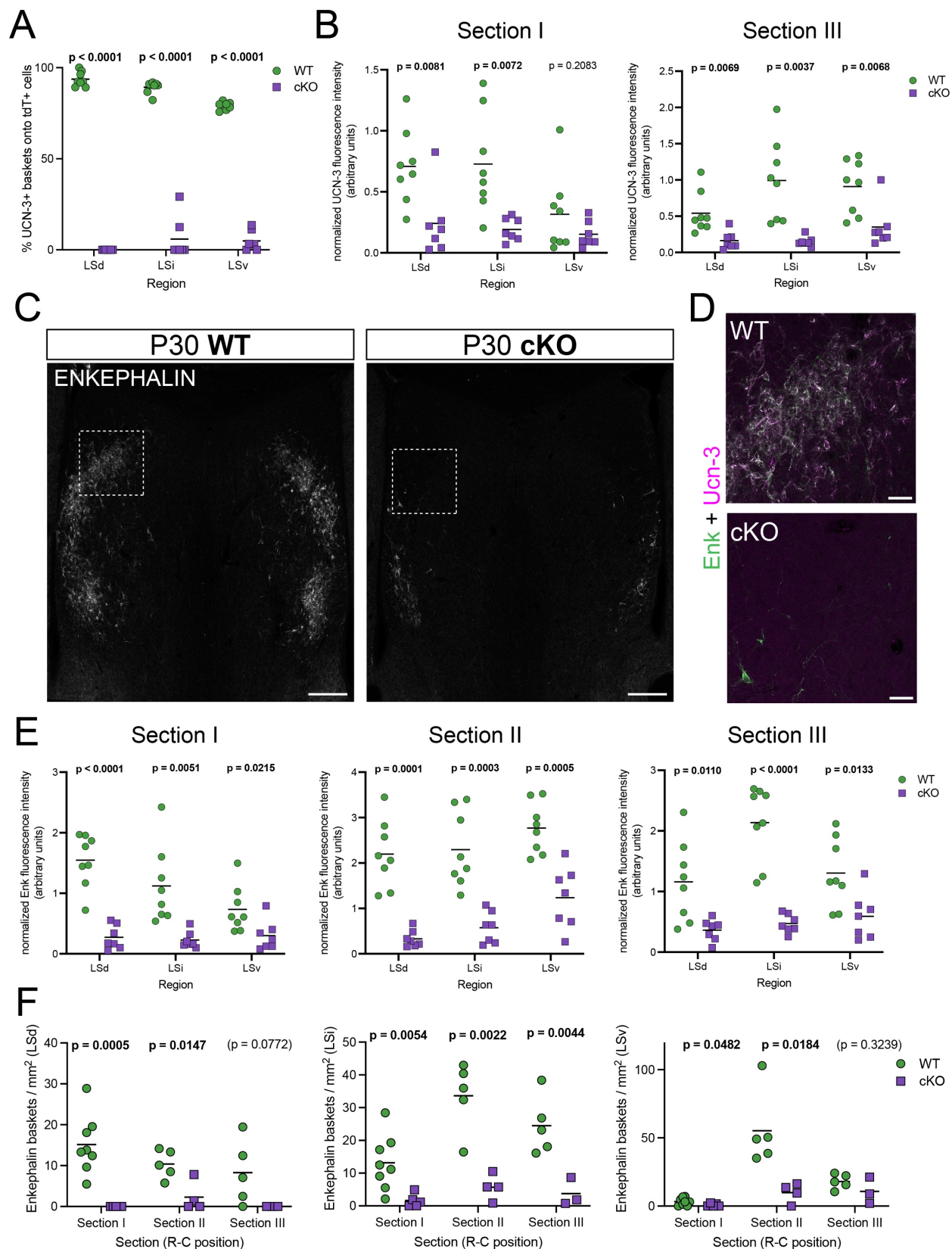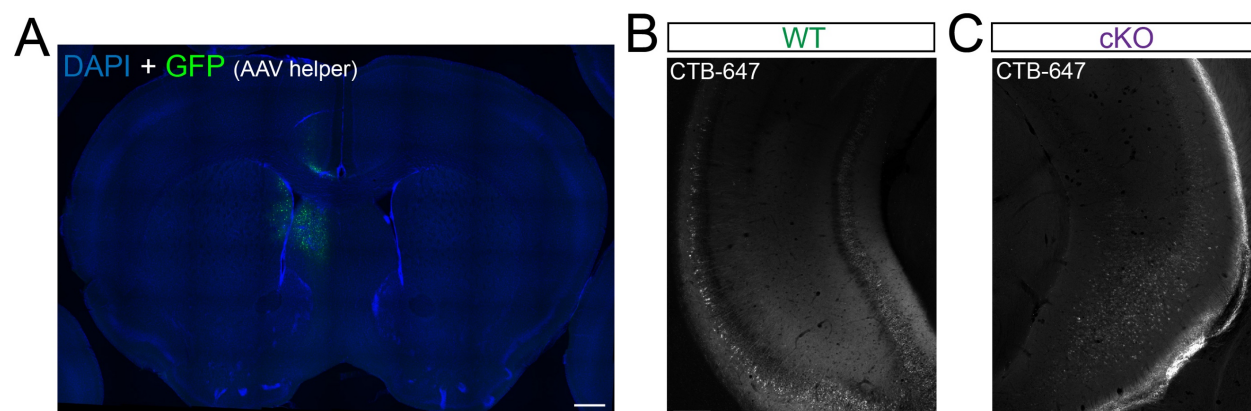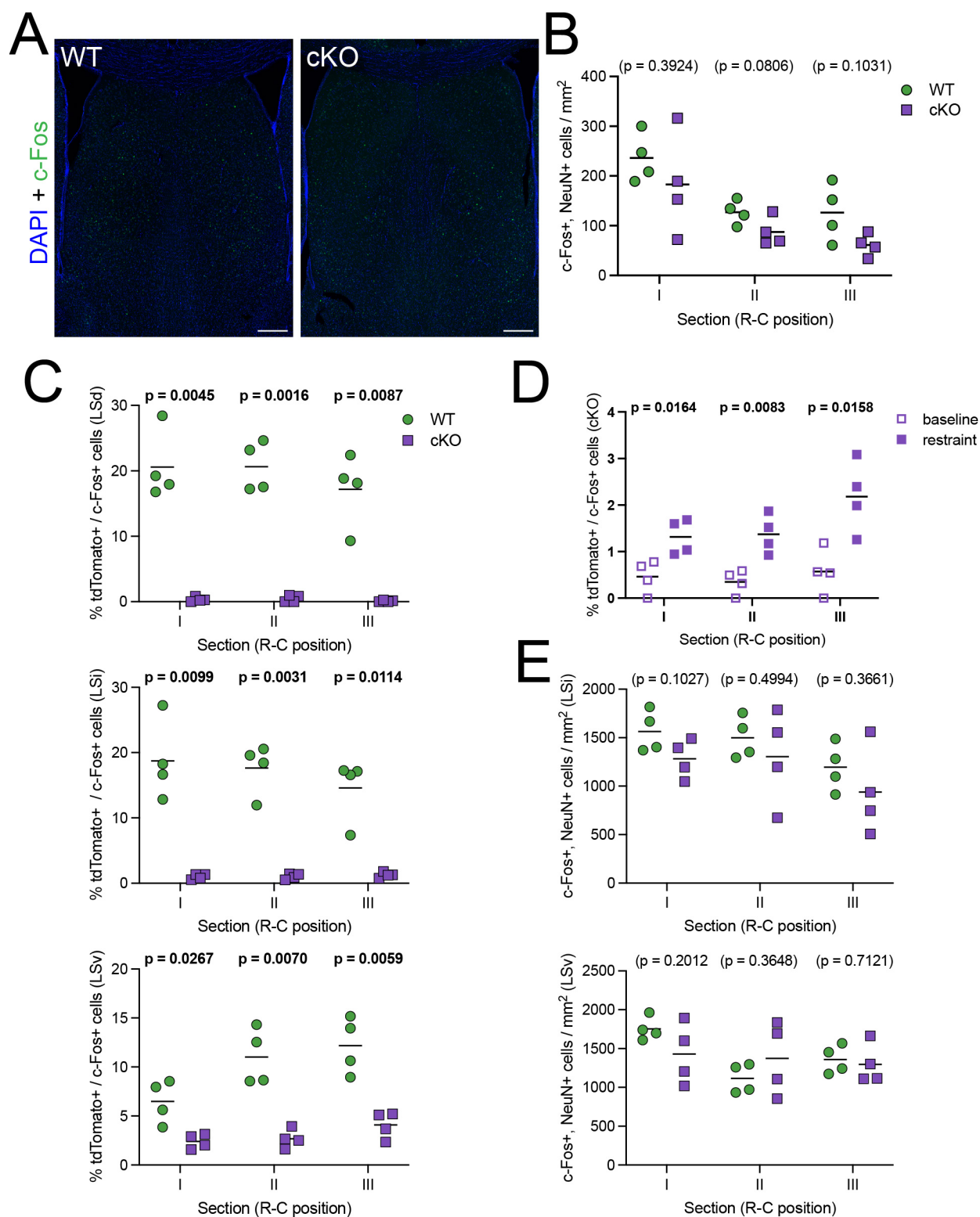
# Figure S1

# Figure S2

# Figure S3



**A** DAPI + GFP (AAV helper)

**B** WT — CTB-647

**C** cKO — CTB-647

# Figure S4

# Figure S5